ELSEVIER

Journal of Nuclear Materials 265 (1999) 178–202

journal of nuclear materials

Synergistic effects of LiOH and F^- in accelerating the corrosion of Zircaloy-4

Y.-M. Wong [a], B. Cox [a,*], N. Ramasubramanian [b], V.C. Ling [c]

[a] *Centre for Nuclear Engineering, University of Toronto, 184 College Street, Toronto, Ontario, Canada M5S 3E4*
[b] *Ontario Hydro Technologies, 800 Kipling Ave., Toronto, Ontario, Canada M8Z 5S4*
[c] *Atomic Energy of Canada Ltd., Chalk River Laboratories, Chalk River, Ontario, Canada K0J 1JO*

Received 2 February 1998; accepted 10 August 1998

Abstract

During prolonged autoclave testing of Zircaloy-4 fuel cladding batches at 360°C major excursions in the corrosion rate occurred when additional unautoclaved pickled specimens were added to autoclaves operating with pH12 LiOH, but not for those operating with pH7 water. Only specimens from one batch of cladding (D) that had been given an ($\alpha + \beta$) anneal survived unscathed. The possibility that these excursions arose from an effect of enhanced hydrogen content or enhanced fluoride content of the solution arising from the addition of fresh specimens (only some of which were pickled in HNO_3/HF solution) was tested. No evidence for a significant effect of either hydrogen or oxygen overpressure was observed if freshly pickled specimens or fluoride were not added to the autoclave. The deliberate addition of fluoride (but no addition of specimens) to the autoclaves once the initial specimens had reached their rate transition resulted in a large corrosion rate excursion for the specimens operating in pH12 LiOH with a hydrogen overpressure, but not for those operating with an oxygen overpressure. Examination of specimens that had undergone accelerated corrosion following F^- additions to autoclaves operating with pH12 LiOH and hydrogen overpressures showed that some specimen surfaces were covered with arrays of blisters. Sections through these oxide films showed a morphology similar to incipient spalling of oxide observed on PWR fuel cladding. The oxides appeared to have delaminated to create the blisters. SEM studies showed collections of large equiaxed oxide or oxyfluoride particles a few μm in size inside these blisters. The presence of large oxide single crystals embedded within cracks in the oxide, the fracture cross sections and features observed at the oxide/metal interface suggested that an hydrothermal oxide dissolution and redeposition process was responsible for the accelerated corrosion. SIMS profiles showed a high uniform F^- content throughout the bulk of the oxide of specimens undergoing accelerated oxidation, whereas the F^- content of an oxide grown with a high oxygen overpressure was less than the oxide on a pickled specimen grown in LiOH solution alone. The high oxygen overpressure may be capable of oxidizing F^- from the solution thus preventing the synergistic effects of LiOH and F^- from accelerating the corrosion of these specimens.

1. Introduction

The possibility that concentration of LiOH in zirconium oxide films under severe thermal hydraulic conditions might lead to enhanced cladding corrosion [1] has led to the almost routine testing of PWR cladding alloys in a range of concentrated LiOH and boric acid solutions [2–5]. In general such tests in laboratory autoclaves have not shown any severe acceleration of post-transition corrosion rates unless the LiOH concentration was increased to $\geqslant 0.1$M LiOH (pH13) during tests in the absence of boric acid [6–8]. Exceptions appear to be restricted to Zr–Nb alloys, where even under constant low LiOH concentrations in-reactor some sudden accelerations of the corrosion rates have been observed [9], and to occasional corrosion rate excursions during

* Corresponding author. Tel.: +1-416 978 2127; fax: +1-416 978 4155

0022-3115/99/$ – see front matter
PII: S0022-3115(98)00507-8

testing of Zircaloys at relatively low LiOH concentrations (Ref. [10], Fig. 4). With the current trend to wider use of Zr–Nb alloy cladding in PWRs the potential for such sensitivity bears watching.

A sharp increase in the corrosion rates of zirconium alloys with increasing LiOH concentrations has long been known to occur for solutions of LiOH with concentrations between 0.1 and 1.0M (pH13-14) [11–15]. These effects are a function of the properties of aqueous LiOH solutions since no such effect occurs with aqueous solutions of any other Li salt [12] or in fused LiOH [16]. Similarly the effects cannot be ascribed to the pH of the solution since at an equivalently high pH, that would cause severely accelerated corrosion in LiOH, only minor increases in corrosion are observed in NaOH, almost no effect is seen for Zircaloys in KOH, and higher alkalis and NH_4OH have no effect [11]. This behaviour has been related to the dissolution and redeposition of ZrO_2 in concentrated LiOH solutions [6–8], and to the known hydrothermal dissolution effects of the different alkalis on tetragonal (or cubic) ZrO_2, compared with monoclinic ZrO_2, at higher temperatures than those used for testing reactor fuel cladding [17].

An initial search for evidence of oxide dissolution during exposure of Zircaloy specimens in concentrated LiOH solutions [18] was inconclusive as no recognisable surface features on the oxides (that were clearly a result of a dissolution process) could be established, primarily because the original appearance of the same area of surface was not known. A subsequent study where the initial surface features were carefully characterised, and the same area of surface was studied after each exposure to LiOH solutions (with or without boric acid additions), led to the conclusion that an hydrothermal dissolution of t-ZrO_2 locally to give pores, with the redeposition of m-ZrO_2 elsewhere, was the cause of the enhanced corrosion of zirconium alloys in concentrated LiOH solutions [6–8,19]. The characteristic feature of oxide films that have been degraded in this fashion in-reactor appears to be the presence of large equiaxed oxide crystallites that are unstable in the electron beam of the electron microscope [20–22].

The only other chemical species known to cause severe degradation of zirconium oxide films when present in high-temperature water in low concentrations is fluoride ion [23–27]. Fluoride is produced in small quantities from a nuclear reaction in-reactors. Until recently the mechanism of this form of degradation had not been investigated. A study of this effect by deliberately contaminating the Zircaloy surface by a delay in the rinsing of the pickling solution has shown that this enhanced corrosion also appears to result from an hydrothermal dissolution and redeposition of ZrO_2 in the presence of fluoride [28]. The result is a mixture of zirconium oxide and oxyfluoride crystallites in the very friable oxide films produced. The characteristic appearance of these oxides is of layers of large oxide platelets lying more or less normal to the oxide/metal interface and oriented parallel to crystallographic directions in the underlying metal grains. Topographical features of the original metal surface were still visible on the oxide surface with only a few small crystallites deposited on top of the original surface. Thus, the hydrothermal processes leading to the growth of the large oxide platelets must have been going on within the oxide film itself.

This paper presents a summary of the results of some autoclave tests during which corrosion rate excursions occurred and of the examinations of the oxide films formed. A mechanism for the apparently synergistic effects of LiOH and fluoride in these tests is proposed. It was expected from the previous experience noted above that an hydrothermal dissolution process had again been at work, but there were characteristic differences in specimen appearance from those observed previously, especially the formation of blisters on some specimens, that appeared to be very similar to end of life oxide blistering on reactor fuel cladding [29].

2. Experimental

2.1. Autoclave testing

Material from 16 different batches of standard Zircaloy-4 cladding were supplied by NFIR [1] members for the initial round of autoclave testing and a further 9 batches (second-round) were added later for a total of 25 NFIR batches. 8 other batches of PWR cladding were also being tested as part of another programme at the same time. Specimens were usually 1 cm lengths cut from these tubes and chemically polished in the standard mixed nitric/hydrofluoric acid chemical polishing solutions. A few 5 cm long specimens were tested in order to examine whether any significant effects from the cut ends of the specimens were present. Specimens were tested at 360°C (633 K) into 2 litre static autoclaves, one of which was operated in pH7 water and the other in pH12 LiOH (both pHs being measured at room temperature). Because of the effects of acid rain on the distilled water supply of the laboratory the water required neutralising with very small additions of LiOH to get pH7. It was in effect, therefore, a very dilute $LiNO_3$ and Li_2SO_4 solution. It is known that the presence of these lithium salts in the water does not affect the corrosion rates of zirconium alloys [12]. Autoclaves were degassed during start-up. Analyses only of those batches of cladding selected to illustrate the observed behaviour are given in Table 1. Of these most were tested in their as-received

[1] Nuclear Fuel Industry Research group, managed by Electric Power Research Inst., Palo Alto, CA.

Table 1
Chemical analyses and post-transition corrosion rates of Zircaloy-4 batches

Batch	D	E	F	H	K	L	M/N	O	P	Q	R	S/T	V
Analyses (ppm, *wt%)													
Sn*	1.45	1.52	1.54	1.62	1.51	1.47	1.54	1.54	1.54	1.54	1.54	1.21	1.53
Fe*	0.226	0.200	0.182	0.222	0.200	0.198	0.227	0.227	0.227	0.227	0.227	0.218	0.210
Cr*	0.111	0.106	0.101	0.105	0.093	0.094	0.103	0.103	0.103	0.103	0.103	0.104	0.110
H	5	18	10	15	11	7	14	10	11	10	7	8	7
O	1210	1143	1250	1085	1021	1156	1070	1200	1200	1100	1100	1550	1200
N	31	29	34	41	46	37	20	30	30	18	18	15	35
C	160	175	130	105	60	115	123	123	123	123	123	130	140
Al	70	<35	<35	59	<35	<35	–	–	–	–	–	–	–
Si	77	76	93	73	113	<25	–	–	–	–	–	–	
Ni	37	30	36	28	<25	<25	–	–	–	–	–	–	
Corrosion rates (mg/dm^2 day; pickled specimens)													
pH7; 1000 days	0.44	0.34	0.82	0.36	0.35	0.69	0.59 [a]	0.45 [a]	0.47 [a]	1.13 [a]	0.96 [a]	0.29 [a]	0.35 [a]
pH12; 350 days	0.82	0.97	1.77	0.98	0.55	1.72	–	–	–	–	–	–	–
Metallurgical condition	RXA	RXA	β-q	SRA	RXA	Low-ΣARXA		SRA	RXA	β-q	β-q	Low Sn SRA	SRA

[a] At ~850 days.

metallurgical condition. Several batches were also tested after a 1 h, 600°C anneal in vacuo, and one batch (D) was also tested after an (α + β) anneal and slow cool (to simulate a weld heat affected zone). Another batch of large diameter guide tube (E) had its wall thickness reduced by machining so that oxide induced stresses would be greater. Details and analyses of all the batches involved can be found in reference [30].

When the additional batches of specimens were added, in addition to pickled specimens, specimens with the as-received belt-ground finish on the outside and a pickled inside (OSAR/ISP), and fully electropolished or flash-electropolished specimens were included. Thus, only half of the added specimens had been exposed to the mixed nitric/hydrofluoric acid chemical polishing solution, whereas all the 'first-round' specimens had been so treated. Because of the large number of additional specimens two more autoclaves were used, one operating in pH7 water and the other in pH12 LiOH. In order to allow for possible minor differences in behaviour in different autoclaves, of the triplicate sets of specimens, two were placed in the extra autoclaves, and one of each set of three was added to the already operating autoclaves.

This addition of new 'second-round' specimens to the already post-transition first-round specimens resulted in an excursion in the corrosion rates of these specimens in the pH12 LiOH, but not in pH7 water. No evidence for either a temperature transient, or leakage of the autoclave (that could have concentrated the LiOH) was found. All specimens showing high weight gains (>250 mg/dm^2) as a result of the excursion were removed, and the remaining specimens (together with those from the extra autoclave operating with pH12 LiOH) were combined in one autoclave. A further corrosion rate excursion occurred during the next operating cycle and resulted in high weight gains for essentially all remaining specimens. Only the specimens given the (α + β) anneal survived. The pH12 LiOH tests were then terminated. Similar additions of new specimens to the pH7 water test, and subsequent combination of all specimens into one autoclave (after removing some specimens for hydrogen analyses) gave no indication of causing any disturbances to the nearly linear post-transition corrosion rates.

In order to investigate the causes of the corrosion rate excursions autoclave tests were started with freshly pickled or abraded specimens in pH12 LiOH. Some autoclaves were operated with up to 200 psig (1.3 MPa) hydrogen overpressure and others with similar oxygen overpressures. Earlier studies [31] had shown higher corrosion rates in pH14 LiOH with oxygen overpressures than with no overpressure (although the corrosion process would have generated a hydrogen overpressure in the latter). No major effects of the hydrogen or oxygen overpressure were observed in these tests where fluoride contamination of the environment was low because of the small number of specimens in the autoclaves. Some batches showed slightly higher corrosion rates with H_2 compared with O_2 overpressures, while some showed the reverse. No batches showed major corrosion rate excursions after the transition in the oxidation kinetics, irrespective of whether they were initially pickled or abraded.

Another cause of the excursions that was considered to be highly probable was a synergistic effect of LiOH and fluoride leached from the fresh specimens added to the autoclaves. In order to test this, autoclave tests were started with hydrogen overpressures of either 50 or 200 psig (0.3 or 1.3 MPa) and oxygen overpressures of either 50 or 200 psig (0.3 or 1.3 MPa). Specimens were initially pickled in the normal manner and oxidized in pH12 LiOH for a total of 90 days, by which time previous evidence showed that they would just have reached the kinetic rate transition. Specimen numbers were again small so that contamination from the pickled surfaces was insufficient to cause any effect. At this point 100 ppm fluoride in the form of depleted, neutralised, chemical polishing solution was added. This solution was prepared by adding a Zircaloy sample to a small, known volume of the standard 50% HNO_3(70%); 5% HF(48%); 45% water pickling solution and leaving it at ~60°C until all reaction had ceased. The remaining Zircaloy was removed, the solution was neutralised with LiOH, and decanted. The amount of solution added to the autoclave tests was calculated from the original fluoride content of the solution, with no allowance made for fluoride deposits on the surface of the remaining Zircaloy specimen or in the material left behind after decanting. The 100 ppm F^- value therefore represents an upper bound. In addition $LiNO_3$ at a concentration of ~1000 ppm will have been added as a result of neutralising the nitric acid remaining. No effect of this addition would be expected [12].

The autoclave tests were then continued for a further 30 days when it was observed that a major corrosion rate excursion had been induced in the autoclaves operating with hydrogen overpressures while no excursion was apparent for specimens in the autoclave operating with a high oxygen overpressure. A small effect was evident in the autoclave with the low oxygen overpressure. No further examination of any specimens was undertaken at this time.

During the testing procedure the autoclave cycle time was varied to minimise the number of shutdown and start-up cycles. Initially fresh specimens were exposed for 7 or 14 days; the cycle was increased to a 28–30 day cycle after a total of 28 days; subsequent cycles of about 60 days began after most specimens had passed through transition (~140 days); finally, the cycle was increased to 120 days after a total exposure time of ~600 days. There was some interest in seeing whether the number of thermal cycles affected the kinetics, so, when fresh samples were added to the system the extra autoclaves needed were operated on ~30 day cycles ('short-cycle' specimens), while the specimens added to the already operating autoclaves (then on '60 day' cycles) saw only 60 and 120 day exposure cycles ('long-cycle' specimens). Reactor fuel cladding, under ideal conditions, is examined at a minimum of every ~360 days so that it may see very few thermal cycles compared with specimens tested in autoclaves.

2.2. Specimen examination

Specimens were selected from those that had undergone spontaneous corrosion rate excursions in 360°C, pH12 LiOH and from those caused to degrade by deliberate fluoride additions. Generally specimens were selected from batches that showed the greatest and the least impact of excursions on their corrosion rates. Oxide thicknesses were established from the specimen weight gain and FTIR interferometry [32], and the extent of porosity was established from impedance measurements during immersion in 1M ammonium nitrate electrolyte [33]. Impedance spectra were taken once the saturation of the oxide with the electrolyte had reached equilibrium.

Specimens were examined by optical and scanning electron microscopy (SEM). The caps of blisters on the surfaces of the worst corroded specimens were removed using sticky tape. This permitted the SEM examination of both surfaces and the other contents of the blisters. Specimens were sectioned metallographically, after being wrapped in zirconium foil to prevent the fracturing of the blisters. The metal substrate was then dissolved away with etching solution to allow SEM examination of the oxide/metal interface topography of the oxides [34]. The stripped oxide films were glued to a glass plate and fractured [35], the fractured surfaces were examined by SEM. Small pieces of the stripped oxide were collected and ion-milled (Gatan 600) from the oxide/environment side to produce oxide foils close to the oxide/metal interface that were transparent enough for transmission electron microscopy (TEM). Success in thinning transverse sections of oxides with the equipment available still remains elusive. The foils were examined in bright and dark field to study the crystallite size near the oxide/metal interface using either an Hitachi (H800) or a JEOL (EM430) TEM. Diffraction patterns were compared with data from the International Crystallographic Index of Structures.

3. Results

3.1. Autoclave testing

Figs. 1 and 2 show the general behaviour of selected specimens in pH7 water and pH12 LiOH during the initial testing. The points at which fresh specimens were added, or the contents of two autoclaves were combined are indicated on these figures. No perturbation of the smooth curves was evident in pH7 water, whereas the excursions induced by specimen additions in pH12 LiOH are clearly seen. It is interesting to note that the

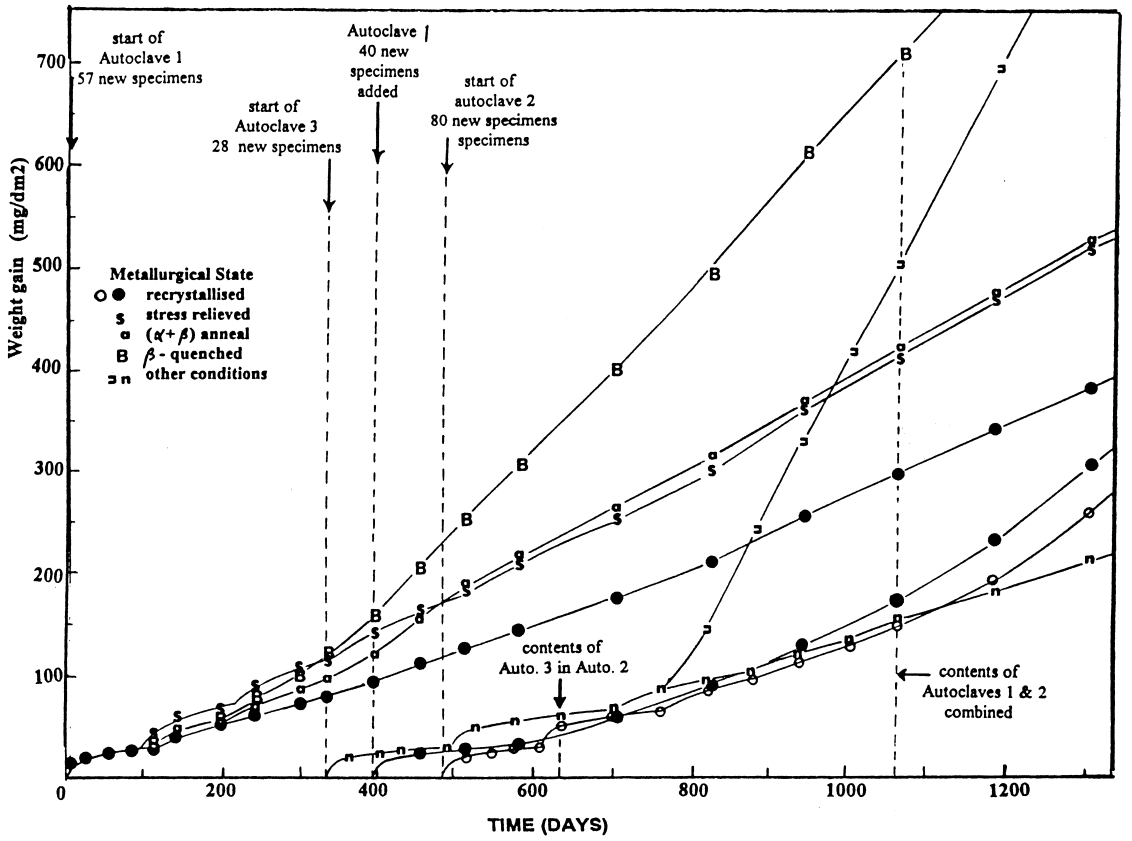

Fig. 1. Sequence of specimen additions to a 1300 day corrosion test in 360°C, pH7 water.

first addition of a small number (28) of fresh specimens at 280 days to the pH12 LiOH test did not cause an excursion, only the later additions of larger numbers. This first group of added specimens had 50% belt-ground and 50% pickled surfaces.

Fig. 3 shows results in pH7 water for an initially RXA batch of cladding (D). An α-anneal reduced the post-transition corrosion rate significantly, and an (α + β) anneal and slow cool resulted in a post-transition corrosion rate not significantly different from that of the original material. The post-transition kinetics showed slowly increasing rates similar to those reported by Peters [36]. No effect of specimen length (1 or 5 cm) was found indicating that specimen ends were not oxidising at a significantly different rate from specimen faces. This batch, in the (α + β) annealed condition was the only one that did not show an oxidation excursion when new specimens were added (Fig. 3). Prior to the excursion the (α + β) annealed specimens corroded less than the as-received specimens, an unexpected result.

Prior to the major oxidation rate excursion the corrosion behaviour of RXA material (batch K) in pH12 LiOH was identical to that in pH7 water during the early pre-transition oxidation period (Fig. 4), transition occurred earlier in pH12 LiOH than in pH7 water, and post-transition corrosion rates were a factor of about two higher in pH12 LiOH than in pH7 water. For a β-quenched batch (F) there were increases in rate for pH12 compared with pH7 conditions even in the pre-transition period, a reduced time to transition, a higher ratio of post-transition rates (pH12 rate $\geqslant 4$ times pH7 rate), and much more scatter between nominally identical specimens (Fig. 5). Because of the increased scatter between duplicate specimens in pH12 LiOH a clear effect of specimen thickness was not evident for batch E specimens.

No reliable results on the effects of surface preparation on corrosion in pH12 LiOH were obtained because it was the addition of these specimens that triggered the corrosion rate excursion. Insufficient steady-state corrosion data were obtained from the specimens in the separate autoclaves to allow trends to be well established. However, in general, all surface preparations behaved worse during this first 60 days than expected from the first-round results. The effects of small oxygen and hydrogen overpressures on the corrosion rates in pH12 LiOH were also small. Although there was some scatter in the behaviour of

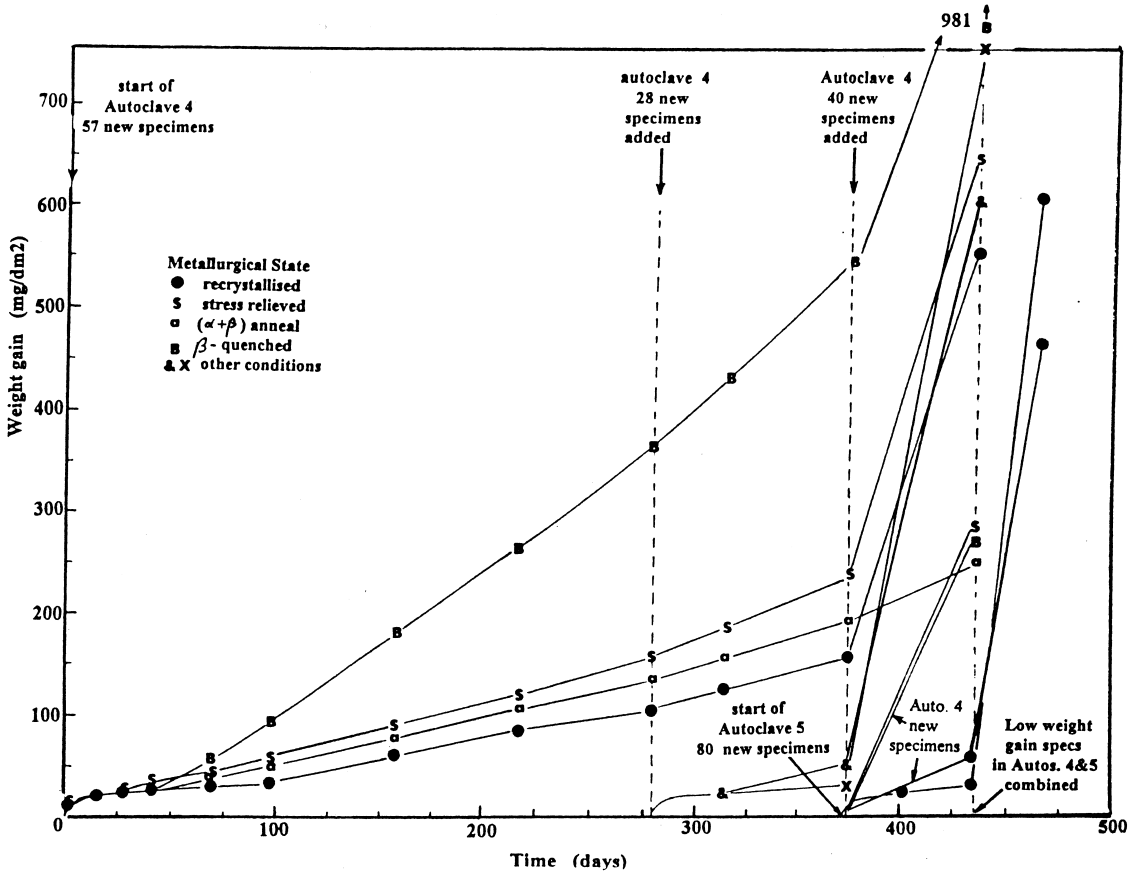

Fig. 2. Sequence of specimen additions to a 437 day corrosion test in 360°C, pH12 water.

some batches, an example using a low ΣA batch (L), that gave generally poor corrosion resistance, shows the results for both oxygen and hydrogen overpressures lying within the scatter for the earlier experiments where the autoclaves were degassed (Fig. 6). Some typical results of the transients induced by adding fresh specimens to the already operating tests are shown in Fig. 7 for an SRA Zircaloy-4 (batch H) and in Fig. 8

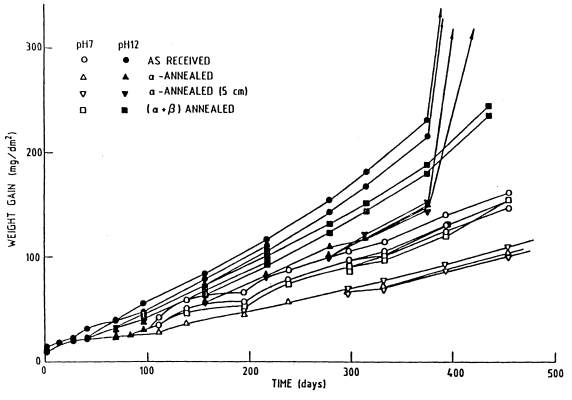

Fig. 3. Effect of α-annealing and an (α + β) anneal and slow cool on the corrosion of RXA Zircaloy-4 (batch D) in 360°C, pH7 and pH12 LiOH.

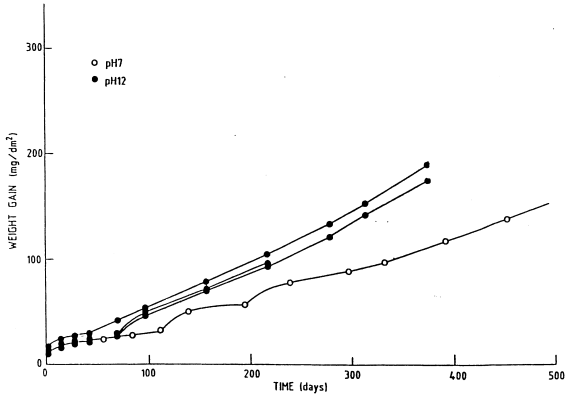

Fig. 4. Small differences in post-transition corrosion and earlier onset of transition in pH12 LiOH compared with pH7 water (RXA Zircaloy-4, batch K).

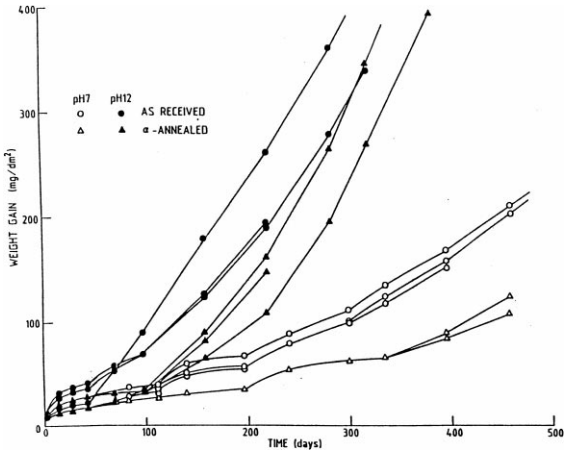

Fig. 5. Large differences between behaviour in pH12 LiOH and pH7 water for a late β-quenched Zircaloy-4 (batch F).

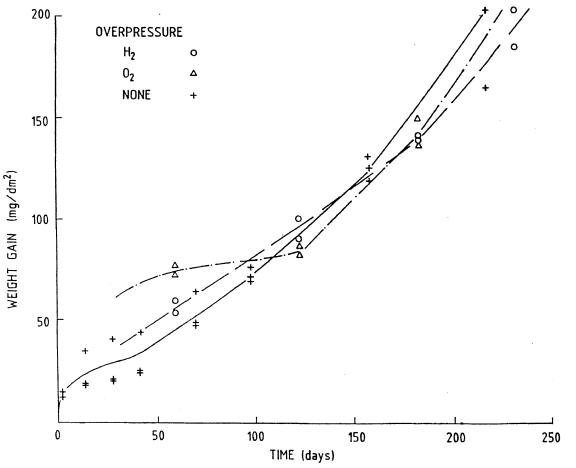

Fig. 6. Effect of H_2 and O_2 overpressures on oxidation of SRA Zircaloy-4 (batch L) in pH12 LiOH at 360°C.

for a β-quenched batch (F). Essentially all batches responded similarly during the last 60 days exposure and showed weight gains that doubled or tripled during this period. They did not appear to be affected when a smaller number of freshly pickled specimens were added at 280 days and the next exposure lasted only 30 days. The one exception was the (α + β) annealed and slow cooled group of specimens from batch D (Fig. 3). All other conditions of this batch of material underwent transients.

The transients induced by deliberately adding fluoride to pH12 LiOH solutions are shown in Fig. 9 for a batch of RXA Zircaloy-4 (batch M), in Fig. 10 for a late β-quenched batch (R) and in Fig. 11 for a low-Sn Zircaloy-4 batch (S). Corrosion in the autoclave with a 200 psi H_2 overpressure was lower than would be expected from the sequence of results with other hydrogen and oxygen overpressures because of a leak which occurred during the last 30 days exposure. The specimens in this

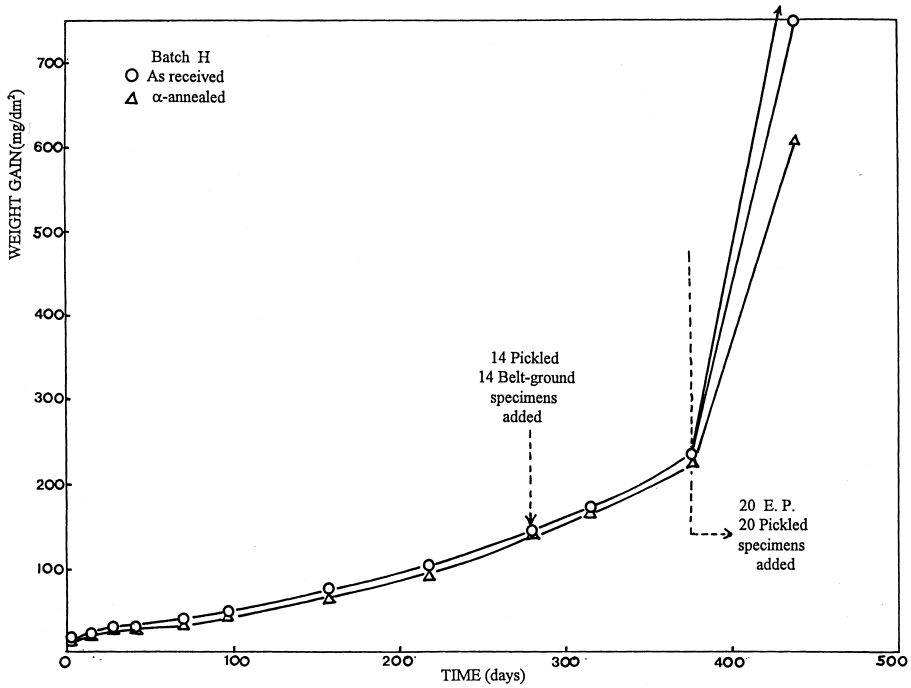

Fig. 7. Effect of adding new specimens (to a pH12 LiOH test) on the corrosion of SRA Zircaloy-4 (batch H).

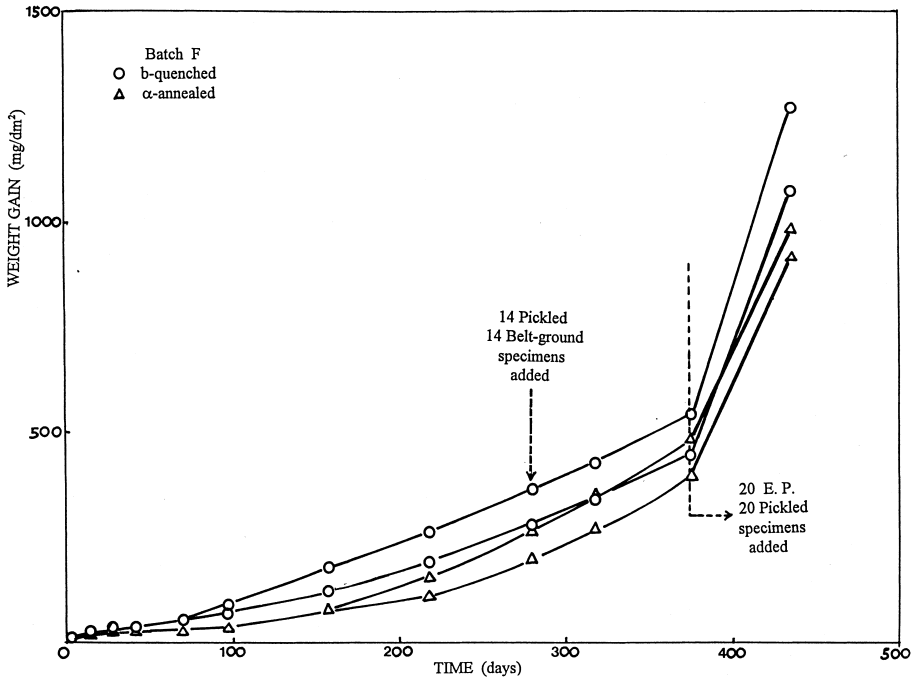

Fig. 8. Effect of adding new specimens (to a pH12 LiOH test) on the corrosion of late β-quenched Zircaloy-4 (batch F).

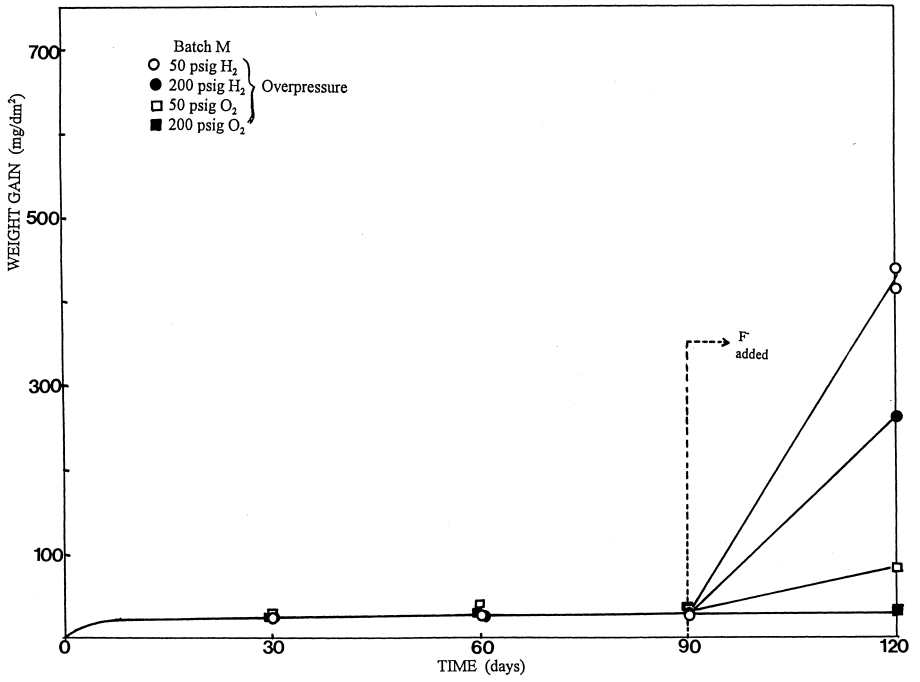

Fig. 9. Effect of hydrogen and oxygen overpressure on the size of the excursion induced by adding F^- to a pH12 LiOH test (RXA Zircaloy-4, batch M).

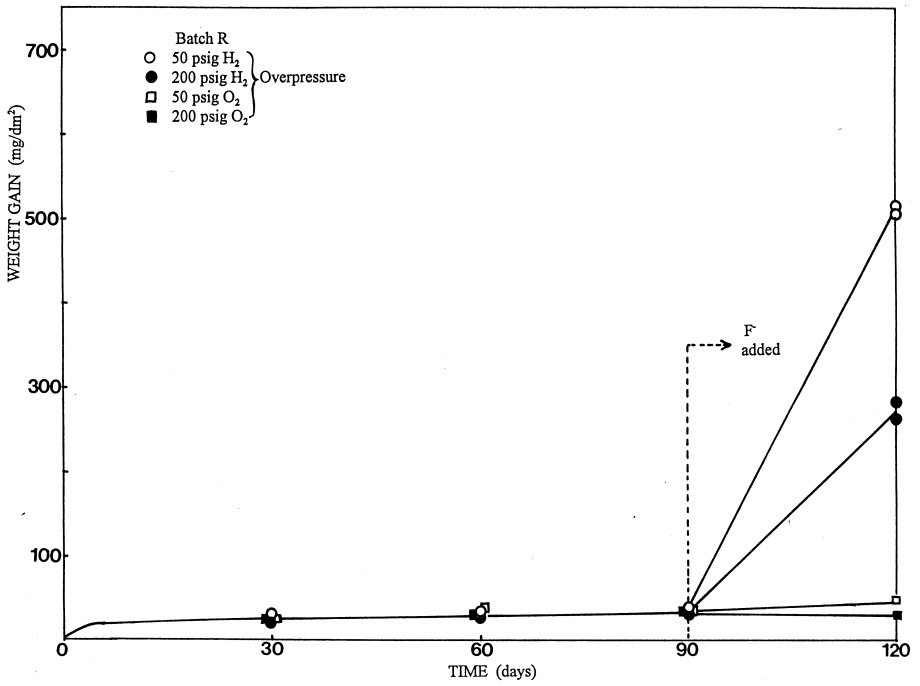

Fig. 10. Effect of hydrogen and oxygen overpressure on the size of the excursion induced by adding F^- to a pH12 LiOH test (late β-quenched Zircaloy-4, batch R).

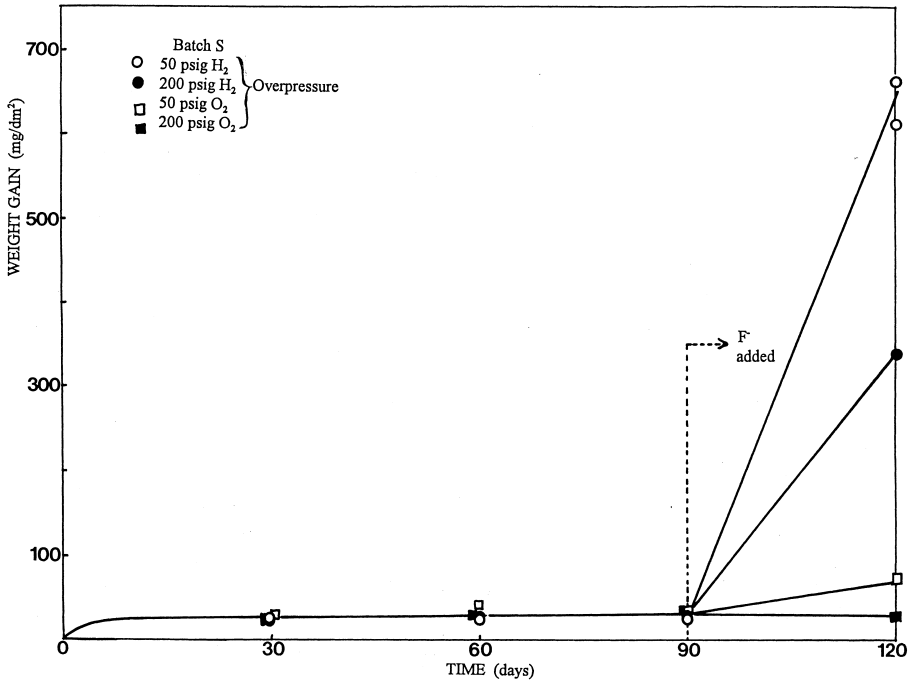

Fig. 11. Effect of hydrogen and oxygen overpressure on the size of the excursion induced by adding F^- to a pH12 LiOH test (low-Sn Zircaloy-4, batch S).

test may not have been in the liquid phase for the whole of the 30 days, and the hydrogen overpressure would have been largely dissipated by the leak.

Hydrogen analyses of the specimens are presented in Tables 2 and 3 and generally showed uptake percentages of 20–25% in both pH7 and pH12 conditions. Uptake percentages after the excursions in pH12 LiOH were slightly higher, and increased with the size of the excursion.

Some minor effects of other variables were noted during the study. Full details are given in Ref. [30], but were excised from this paper at the request of the reviewers. If Ref. [30] is not accessible to readers the authors would be pleased to supply details on request. A brief summary of these effects follows:

- Small increases in corrosion were observed as the wall thickness was reduced. Curves diverged more for oxides >15 μm thick, especially when the wall thickness was reduced below 1 mm.
- Effects of α-annealing generally included longer times to transition and lower post-transition weight gains compared with as-received material. For some batches these differences disappeared at oxide thicknesses >50 μm.
- Effects of surface preparation were negligible for most batches of material (e.g. batch V). For some, however, times to transition were significantly different in the order: full electropolished < flash electropolish < pickled < belt-ground, with differences ranging over a factor of two. At high weight gains the post-transition rates tended to vary little and oxidation kinetic curves were almost parallel (e.g. batch R), except for one batch (M) where the post-transition curves diverged only above ~15 μm oxide.
- A small, but not completely consistent, effect of the autoclave cycle time was evident. Weight gains tended to be less for specimens on the long cycle than for those on the short cycle. Again the post-transition oxidation rates tended to be similar, so that percentage differences declined as oxides got thicker.
- Attempts to extract meaningful corrosion curves for the belt-ground outer surfaces (by correcting for the corrosion of the inner pickled surface using the average corrosion rates of completely pickled specimens) were unsatisfactory because it was observed subsequently (metallographically) that oxide thicknesses on the inner and outer surfaces of pickled specimens were not equal. Post-transition oxidation curves for differently prepared late β-quenched specimens (batch R) were however generally parallel, showing that the effect of surface preparation mainly affected the way in which specimens went through the kinetic rate transition.

3.2. Specimen examinations

Fig. 12 shows an optical micrograph of a typical blistered oxide surface obtained after a deliberate corrosion rate excursion at 360°C with a 50 psi (0.3 MPa) hydrogen overpressure. Specimens from the batches that showed no excursions in the test with a 200 psi (1.3 MPa) oxygen overpressure exhibited thin jet black oxide films.

In general oxide thicknesses calculated from weight gains and FTIR were in good agreement. Differences arose where FTIR spots (~40 μm dia) were placed on blisters; the FTIR thicknesses so obtained were larger than the weight gain thicknesses despite the presence of the empty blister. Internal reflections were not obtained from the rough surface of the bottom of the blister due to scattering, and the interference fringes obtained were therefore attenuated and somewhat irregular in shape. Table 4 gives the oxide thicknesses calculated from weight gain, FTIR and capacitance measurements. Impedance changes during soaking were small for specimens corroded with oxygen overpressures, but large and

Table 2
Hydrogen contents measured for pickled specimens after 1064 days in 360°C, pH7 water

Batch	Met. condition	Wt. gain (mg/dm^2)	H. content	
			(ppm)	(mg/ dm^2)
D	RXA (1 cm)	402	415	7.00
	RXA (5 cm)	285	445	7.80
	RXA (+α. Ann.)	278	389	6.80
	RXA (+(α + β) Ann.)	410	464	8.10
E	RXA (0.04")	269	276	7.10
	RXA (0.03")	288	401	7.50
	RXA (0.02")	318	565	7.10
F	β-q.	703	579	10.40
	β-q. (+α. Ann.)	688	485	9.00
H	SRA	327	404	6.90
	SRA (+α.Ann.)	313	404	7.00
K	RXA	343	417	7.00
L	SRA (low ΣA)	534	582	8.60

Table 3
Hydrogen contents measured for electropolished or belt-ground (inside pickled) specimens in 360°C, pH7 water after 670 days

Batch	Condition		Wt. gain(mg/dm^2)	H. content	
	Met.	Surf.		(ppm)	(mg/dm^2)
L	SRA	EP	321	717	10.20
		OSAR/ISP	253	450	7.00
M	RXA	EP	195	396	5.60
		OSAR/ISP	171	333	5.10
N	RXA	EP	226	459	6.30
		OSAR/ISP	181	378	5.40
O	SRA	EP	237	379	7.10
		OSAR/ISP	198	311	6.05
P	RXA	EP	205	320	6.00
		OSAR/ISP	149	274	5.25
Q	β-q	EP	606	569	8.65
		OSAR/ISP	571	527	8.60
R	β-q	EP	420	384	7.50
		OSAR/ISP	321	322	6.50
S	Low-Sn	EP	176	273	5.20
		OSAR/ISP	141	216	4.20
T	Low-Sn	EP	202	360	5.20
		OSAR/ISP	157	312	4.70
V	SRA	EP	197	310	5.90
		OSAR/ISP	189	276	5.40

rapid for those with H_2 overpressures. Typical capacitance vs. time plots and impedance spectra (after soaking) are shown in Fig. 13. Table 5 gives a list of the frequency dependence of the measured capacitance–reactance responses of the soaked oxides. The hydrogen overpressure specimens in general show two distinct slopes whereas for specimens exposed with oxygen overpressures there was generally one regular slope. The specimens from the original autoclave tests that showed spontaneous oxidation rate excursions generally showed two slopes on the impedance curves.

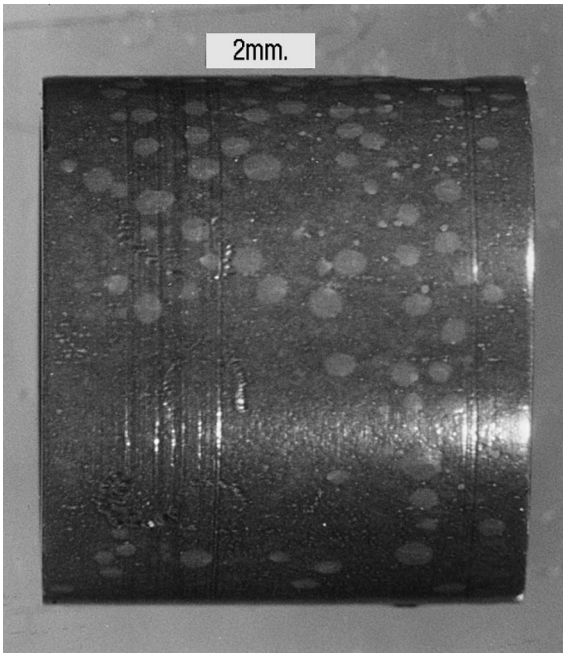

Fig. 12. Optical microscopy at 6x magnification shows severe blistering of the worst specimens autoclaved in LiOH/F^- solution at 360°C with a low hydrogen overpressure (S30).

It can be seen from the fracture cross section (Fig. 14(a)) that the thick oxides are composed of two layers where the bottom layer showed much more porous fracture features. No such differences were seen in oxides not showing rate excursions (Fig. 14(b)). That the upper layer of the oxide was the oxide formed in pH12 LiOH prior to fluoride addition was shown by the presence of surface features clearly derived from the original pickled surface of the specimen (Fig. 15). The appearance of a cross section of a large blister is shown in Fig. 16. The uniformity of the oxide/metal interface beneath the blister indicates that the porosity of the lower oxide layer is unaffected by the presence of the blister. SEM examinations of the underside of a blister cap and the corresponding blister are shown in Fig. 17. The topographical features on the inner surface of the blister cap cannot be matched with the features on the blister interior (Fig. 18) except on the edges where the blister cap broke off. This indicated that changes occurred inside the blister after it was formed. Large equiaxed particles that may be either oxide or oxyfluoride, were found inside some blisters (Fig. 19), and must have been formed there since cracks in the blister cap (prior to removal) were too small for any of these particle to pass through (Fig. 20). It was not possible to obtain samples

Table 4
Oxide thicknesses in (μm) calculated from weight gain, FTIR and capacitance measurements

Overpressure conditions [b]		Δw/15 [d]		FTIR		Capacitance			
		Specimens				I^a	S^a	I^a	S^a
Pressure		Spot#		1	2	1	1	2	2
50	H_2	L30	30	26	26	13.6	6	–	–
50	O_2	L32	6.3	6.3	5.4	6.1	3.9	–	–
200	H_2	L35	20	21	21	12.1	6	9.45	5.25
200	O_2	L36	2.7	3	3.6	2.6	2.4	2.76	2.47
50	H_2	M31	29	34	37	18.4	5.6	15.7	7.11
50	O_2	M32	5.6	8.7	–	4.7	1.9	–	–
200	H_2	M34	18	23	20	6.85	4.8	11.6	8.4
200	O_2	M36	2.5	2.6	–	2.2	2.1	2.23	2.06
50	O_2	P32	5.2	8.9	–	1.7	0.8	–	–
50	O_2	P33	4.2	3.9	2.8	3.75	2	3.5	1.5
50	H_2	R30	34	41	44	13.2	5.2	–	–
50	O_2	R32	2.6	2.6	2.6	1.88	1.6	2.29	2.05
200	H_2	R34	19	24	23	22.3	5.9	10.8	3.62
200	O_2	R36	2	2.7	2.9	2.4	2.2	–	–
50	H_2	S30	41	28	50	18.1	9	21.1	8.68
50	O_2	S32	4.9	5.2	4.8	2.06	1.6	3.66	1.67
200	H_2	S34	23	29	27	14	4.7	13.1	5.99
200	O_2	S36	2.1	2.7	2.7	2.39	2.2	2.31	2
None[c]	–	S16	82.5	99	95	–	2.07	41.53	1.19
None[c]	–	S18	69.4	88.5	73.5	25	3	32.5	5.39
None[c]	–	P4	29.7	32.5	46	18.21	11.3	16.68	9.67
None[c]	–	R4	29.6	46	50	23.6	12.7	–	–

[a] I = Initial reading; S = Saturation value.
[b] 360°C pH12 LiOH + F^-.
[c] Original tests, no deliberate F^- addition.
[d] Δw/15 is the oxide thickness (μm) obtained by the weight gain (mg/dm^2) by 15.

of these particles for diffraction analysis, but they gave the impression of having been deposited from solution.

In an attempt to determine the phases present in oxides that had undergone excursions, some oxide films were stripped and thinned for TEM examination. Obtaining coherent thin oxide sections from the porous oxide near the oxide/metal interface in degraded oxides, proved difficult. However, a few examples were obtained and bright and dark field micrographs and diffraction patterns were obtained from these sections (Fig. 21). The *d*-spacings measured for all the diffraction patterns obtained from these specimens were compared with those for the three phases of ZrO_2 and all reported patterns for zirconium oxyfluorides available in the International Tables (JCPDS-ICDD-1995 available at the Royal Ontario Museum). Principal reflections for oxides and oxyfluorides are often similar because of the relationships between the structures. Only a few characteristic *d*-spacings can be used to clearly differentiate the two. In particular *d*-spacings in the interval 1.9–2.2 Å are typical of oxyfluorides. The measured *d*-spacings on these oxides showed them probably to be a mixture of zirconium oxide and zirconium oxyfluoride crystallites. The crystallite structure is not positive evidence for the operation of a hydrothermal dissolution and deposition process as either zirconium oxide or oxyfluoride crystals can be grown from fluoride solutions depending on the precise chemical conditions [37–39]. The morphology and location of the crystallites are probably better indicators of the formation mechanism.

Evidence of oxide or oxyfluoride crystal hydrothermal growth in the bulk of the oxide was supported by the observation of apparently large fractured crystallites bridging major cracks in the inner oxide (Fig. 22) in the deliberately fractured oxides. These fractured crystallites had what appeared to be river patterns on them suggesting that they were crystalline and not amorphous. The fracture surfaces also showed a few large oxide particles or crystallites within the porous oxide. The oxide/metal interface topography showed no features resulting from the underlying metal structure for specimens that had undergone a corrosion rate excursion (Fig. 23(a)). Prior metal grain boundaries were visible, however, in oxide/metal interfaces of specimens that had not undergone such an excursion (Fig. 23(b)).

Results for the second-round specimens from the original tests that were examined here showed thick porous oxide films (Tables 4 and 5). However, because these specimens had not been exposed to non-fluoridated water conditions, and had therefore not grown an

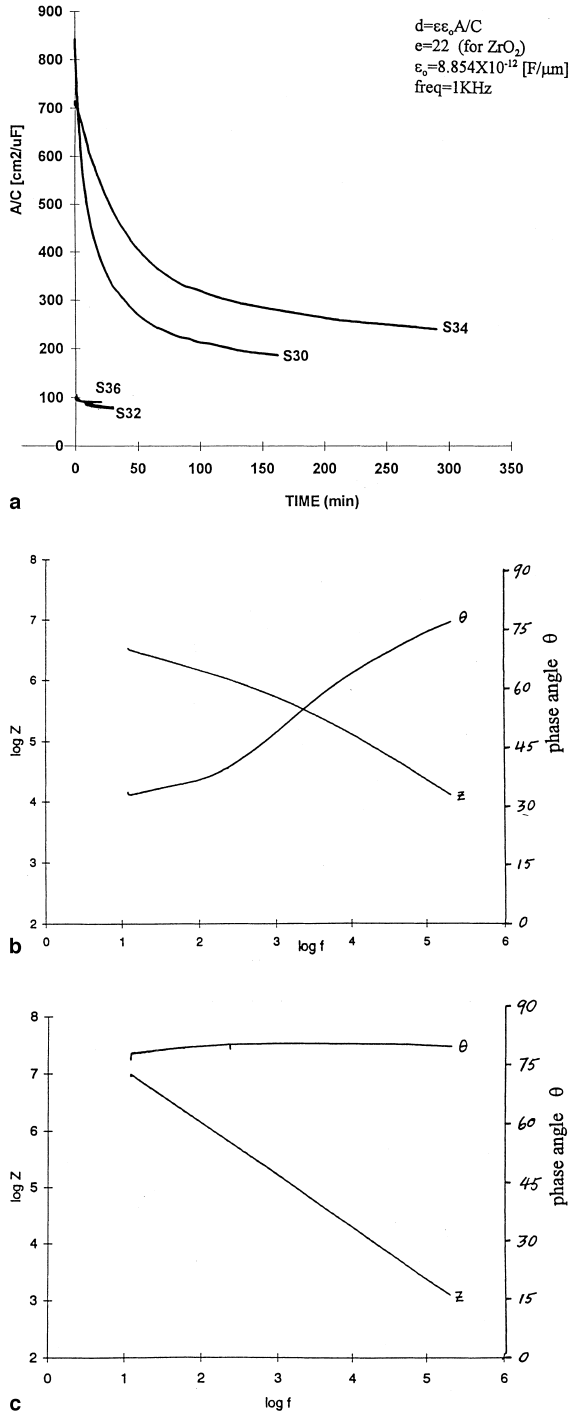

Fig. 13. (a) Capacitance vs time for the low-tin SRA specimens. (b) Impedance spectrum for low-tin SRA specimen oxidised in LiOH solution with a low hydrogen overpressure. (c) Impedance spectrum for low-tin SRA specimen oxidised in LiOH solution with a low oxygen overpressure.

initial normal oxide film, they tended to form thick oxides with radial crack patterns rather than large well defined blisters. This was because there was essentially no normal oxide film of a thickness sufficient to form a coherent blister cap during the rapid growth of the degraded oxide films. There were, however, an array of small 'pustules' on the surfaces of S16 and S18. These were associated with arrays of lateral cracks (Fig. 24).

Secondary ion mass spectrometer (SIMS) profiles through the oxide on specimens that had, or had not, undergone an excursion in corrosion rate were compared with similar profiles for oxides grown in (0.1–1.0 M) LiOH solution without any added fluoride but with the Zircaloy surface initially pickled. SIMS profiles (Fig. 25) showed that there were high concentrations of fluoride throughout the bulk of the oxides that had the excursions, but initially pickled specimens which were not exposed to fluoride during corrosion showed a typically low fluoride concentration except near the oxide surface.

4. Discussion

4.1. Autoclave tests

The most unexpected feature of this testing programme was the large corrosion rate excursions that resulted when fresh specimens were added to autoclave tests in pH12 LiOH in which the original specimens were already in the post-transition region. Similar excursions were not observed in pH7 water, and this 'modus operandi', whereby fresh specimens were added to tests in water or steam, had long been routine, hence the surprise. It was not possible to obtain any similar excursions by changing the hydrogen or oxygen overpressures during tests, however, fluoride additions (without added specimens) produced very similar excursions. With one or two exceptions [9,10], no examples of similar excursions could be found in the literature, although subsequently similar experiences have now become known [40]. No obvious source of fluoride contamination was present in this case, however.

If we are seeing a synergistic effect of LiOH and fluoride ion then why should such an effect of fluoride only become evident when new specimens were added after the rate transition, and not during the initial corrosion of freshly pickled specimens? One contributing factor was probably the large numbers of specimens in these autoclave tests, considerably more than had been the norm in previous tests in LiOH solutions. The second factor, which probably prevented any anomalous corrosion at the start of the tests was the very short (2 days) first autoclave cycle. Thus, initial test periods in pH12 LiOH were 2, 12, 14 days, and with the autoclave cleaned and fresh solution added for each period, much

Table 5
Frequency dependence (slope) of log Z vs. log f obtained from linear least square method

Overpressure conditions			Frequency		Frequency		Frequency		Frequency	
Pressure (psig)	Gas	Spec. spot#	Range (log f) A	Slope	Range (log f) A	Slope	Range (log f) B	Slope	Range (log f) B	Slope
50	H2	L30	3.7–4.8	−0.738	5–5.3	−1				
200	H2	L35	1.08–1.67	−0.553	4.33–5.3	−0.842	1.08–2	−0.537	4.5–5.3	−0.826
50	O2	L32	Full	−1			2.4–3.83	−0.926		
200	O2	L36	Full	−0.96			Full	−0.92		
50	H2	M31	1.08–1.5	−0.327	4.5–5.3	-0.828	1.08–1.7	−0.407	4.5–5.3	−0.866
200	H2	M34	1.25–2	−0.532	4.5–5.3	-0.856	1.25–2	−0.544	4.3–5.3	−0.884
50	O2	M32	1.2–3	−0.926			2.0–3	−0.779		
200	O2	M36	Full	−0.964			1.2–3	−0.961	3.3–5.3	−0.974
50	H2	R30	1.3–1.8	−0.473	4.65–5.3	−0.8	1.08–1.83	−0.505	4.63–5.3	−0.789
200	H2	R34	2.6–3.3	−0.509			1.33–2.2	−0.508	4.85–5.3	−0.828
50	O2	P32					1.75–2.4	−0.759	3.8–5.3	−0.901
50	O2	P33	1.5–3	−0.876	3–5.3	−0.898	1.7–3.7	−0.879	3.8–5.3	−0.879
50	O2	R32	1.25–3.4	−0.957	4.2–5.3	−0.98	3.0–5	−0.947		
200	O2	R36	1.5–4.5	−0.959			Full	−0.959		
50	H2	S30	1.08–1.83	−0.372	4.75–5.3	−0.812	1.6–2	−0.315	4.75–5.3	−0.791
200	H2	S34	1.08–2	−0.542	4.67–5.3	−0.836	1.25–1.88	−0.557	4.5–5.3	−0.835
50	O2	S32	Full	−0.924			1.33–1.66	−0.919	3.17–5.3	−0.907
200	O2	S36	Full	−0.962			Full	−0.972		
None	–	S16	1.25–2	−0.713	4.7–5.3	−0.69	1.25–2	−0.745	4.7–5.3	−0.662
None	–	S18	1.9–2.8	−0.647	4.7–5.3	−0.742	2.6–3.6	−0.685	4.7–5.3	−0.739
None	–	P4	1.08–1.6	−0.594	4.0–5.3	−0.91	1.08–1.5	−0.509	4.5–5.3	−0.9
None	–	R4	1.25–1.6	−0.429	4.25–5.3	−0.866				

Full range from 1.079181 to 5.30103 log scale. (A, B refer to spots A and B, respectively.)

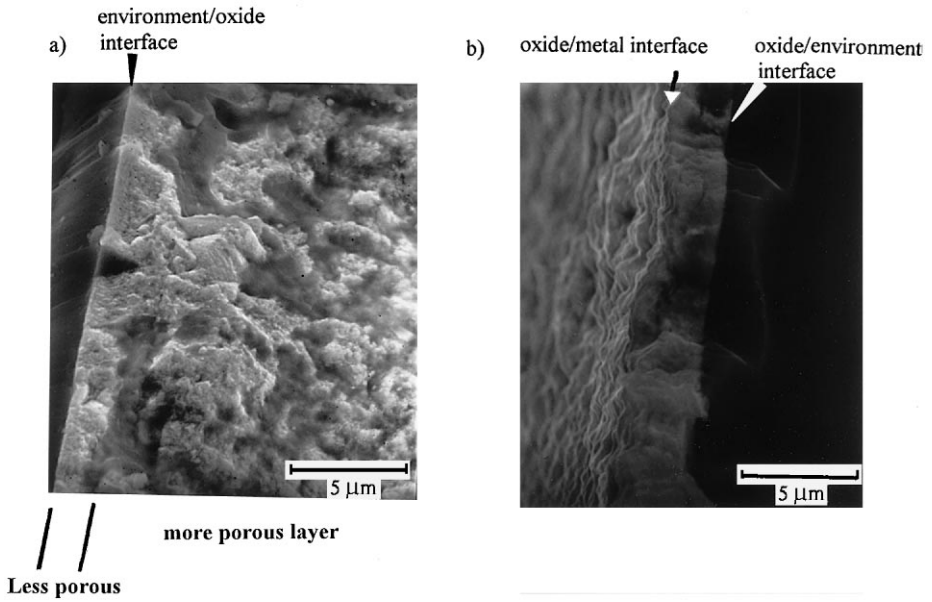

Fig. 14. Fractured cross section of oxide grown in solution with an hydrogen overpressure (a) note that the upper layer (E/O interface) has a much different fracture characteristic similar to (b) the fractured cross section of oxide grown in solution with an oxygen overpressure.

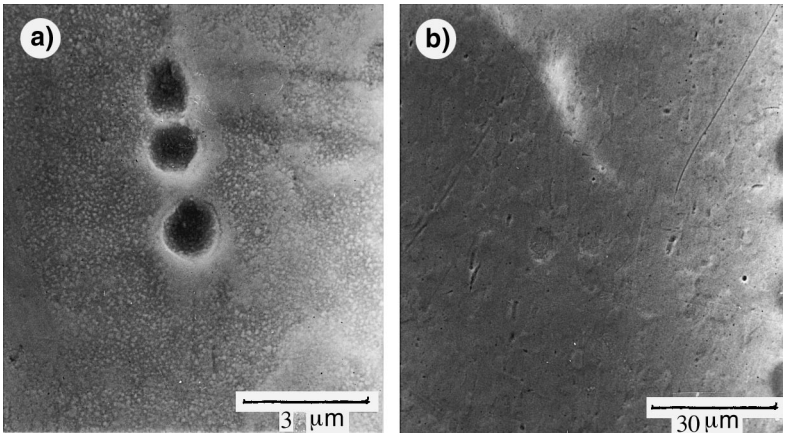

Fig. 15. SEM surface morphology of a specimen oxidised in LiOH/F^- solution with an hydrogen overpressure showing that the preoxidised features of the metal surface were preserved, (a) and (b).

of the fluoride leached from the pickled specimens into the solution was probably removed from the system before serious damage to the initial protective oxide could occur. When the fresh specimens were added during the later stages of the testing the shortest continuous exposure was 30 days, and the worst excursion resulted during a 60 day autoclave cycle. A typical example of the results for these first few cycles is plotted in Fig. 26 for two β-quenched batches of cladding. It can be seen that even in the short initial tests there was probably some increased corrosion in pH12 LiOH compared with pH7 water for the more sensitive β-quenched material, although other batches showed no discernible effect. The shorter the initial operating period the less effect there was on the later pre-transition weight gains for the less sensitive RXA materials. This suggests that the long autoclave operating periods, without changing the solutions, were a major contributing factor and that behaviour in pH12 LiOH of pickled specimens may always be borderline if long initial autoclave cycles were used. This effect of autoclave cycle length, when new specimens are added, coupled with the smaller number of pickled specimens added at 280 days, compared with 376 days, probably explains the absence of an excursion during the 280–310 day cycle. However, it must have been a close call, because possible small accelerations of corrosion rate can be seen for some specimens in Fig. 2 during this cycle. Nevertheless, a synergistic effect of LiOH and F^- was an essential contributor as similar effects were absent from pH7 tests after any of the points where fresh specimens were added and irrespective of the length of the next cycle (Fig. 1).

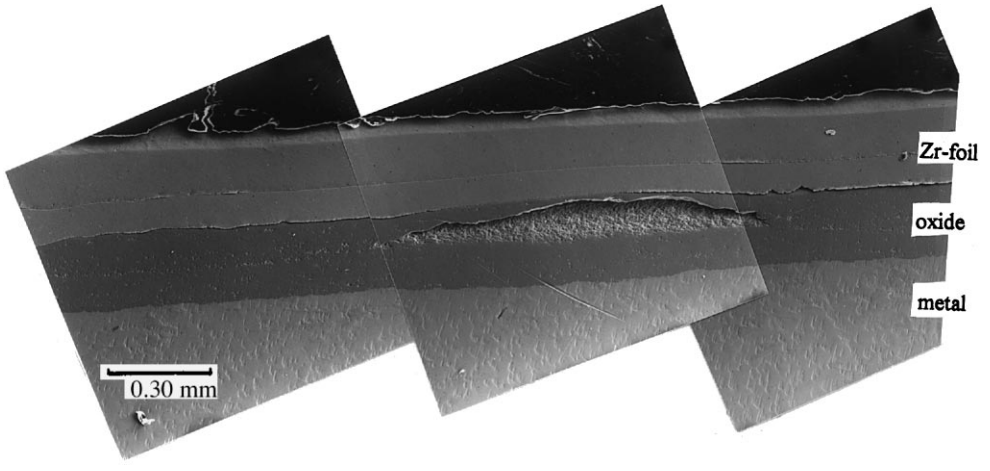

Fig. 16. Cross section of a blistered specimen showing the interior of a large blister, note that the sample was wrapped with two layers of Zr foil (top layers) to prevent the oxide spalling during mechanical polishing.

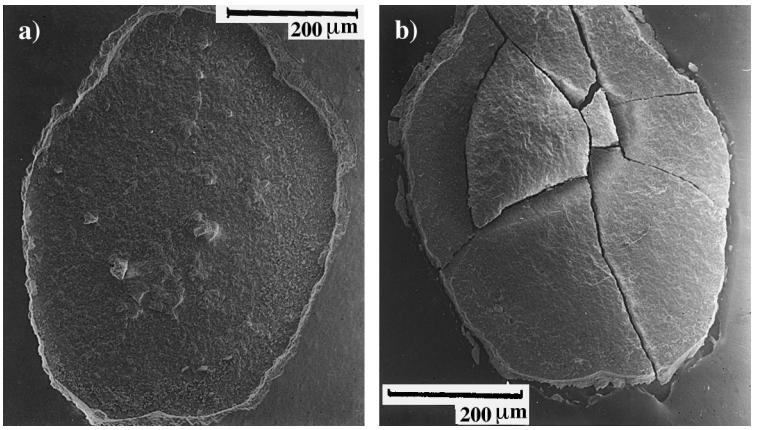

Fig. 17. SEM surface morphology of a blistered specimen (oxidised in $LiOH/F^-$ solution with an hydrogen overpressure) showing the blister interior (a) and the inner face of the blister cap (b).

Other observations during this study were that the pre-transition corrosion rates in pH7 and pH12 solutions were identical for SRA and RXA material, thus demonstrating clearly that Li^+ is not being incorporated into the pre-transition barrier oxide and increasing the oxygen anion diffusion rate in these films. Nor can it be

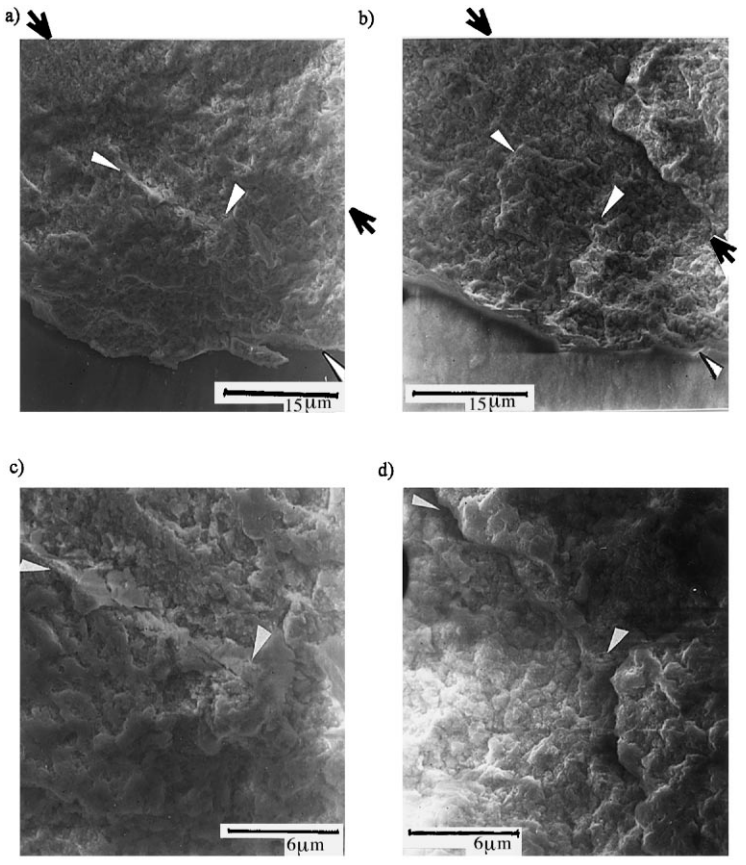

Fig. 18. The opposing surfaces of the blister interior, printed in reverse (b), and its cap (a). The arrows mark the same features on both surfaces. (c) and (d) are the enlarged features marked by the smaller arrows in (a) and (b).

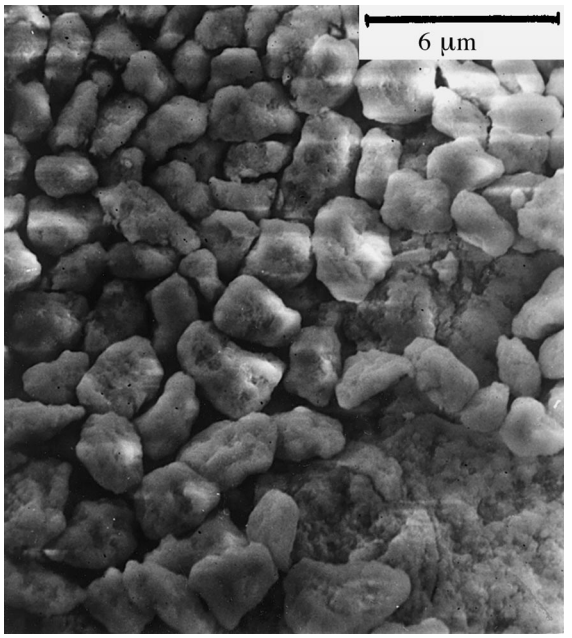

Fig. 19. SEM morphology of particles observed inside initially closed blisters.

modifying the oxide crystallite size in the oxide at this stage in the oxidation process, since such a change would also modify the pre-transition corrosion kinetics as oxide crystallite boundaries are the primary solid state diffusion path for oxygen anions at low temperatures [41,42]. In pH12 LiOH solutions the rate transition occurred at a weight gain only slightly less than that for pH7 solutions. However, because of the approximately cubic kinetics this effectively cuts the time to transition nearly in half.

β-quenched batches of Zircaloy-4, or those with very low ΣA parameters, showed much higher post-transition corrosion rates than either SRA or RXA material in both pH7 and pH12 environments (Table 1). They also tended to show much more scatter between nominally identical specimens, especially in pH12 LiOH (Fig. 5). For most batches of cladding, groups of identical specimens were started in triplicate, with one of the specimens being removed before the end of the test for hydrogen analysis. On all the figures, wherever a single point represents a group of identical specimens, all three weight gains lie within the area of the point. Later, during post-transition corrosion, the spread of the points increased, typically two of the three specimens behaved almost identically while the third one differed significantly. In these circumstances two points are shown on the figure.

Prior to the corrosion rate excursions the post-transition rates in pH12 LiOH were a factor of 2–3 higher than in pH7 water (Table 1). RXA Zircaloy-4 tended to show higher post-transition rates than SRA Zircaloy-4, where the chemistry of the batches was identical. This difference was still evident when all RXA and SRA batches were considered, although the differences were small enough and the spread in behaviour large enough that some overlap in the post-transition rates of the two groups was evident. The low-Sn batch generally gave the lowest post-transition rates, although it seems to have been more sensitive than most, and as sensitive as the worst of the other batches to the processes leading to the corrosion rate transients. Thus, despite the good behaviour of low-Sn batches of cladding under most conditions in-reactor, it might be expected that low-Sn cladding would not show any advantage, and might even be worse than Zircaloy-4 with 1.5% Sn, under very severe reactor conditions that led to early degradation of the cladding corrosion resistance.

Effects of heat-treating the as-received batches of cladding did not result in the expected effects. Thus, a 1 h vacuum anneal at 600°C of batch D material, which was already fairly well recrystallised, resulted in a significant reduction in post-transition corrosion rate in both pH7 and pH12 conditions (Fig. 3), whereas an (α + β) anneal and slow cool, which might have been expected to result in poor corrosion resistance [43] had essentially no effect in pH7 water and gave a small improvement in pH12 LiOH. This treatment, however, apparently rendered the batch immune to the destructive effects of oxide degradation by $LiOH + F^-$. A similar α-anneal of a late β-quenched batch (F) of material

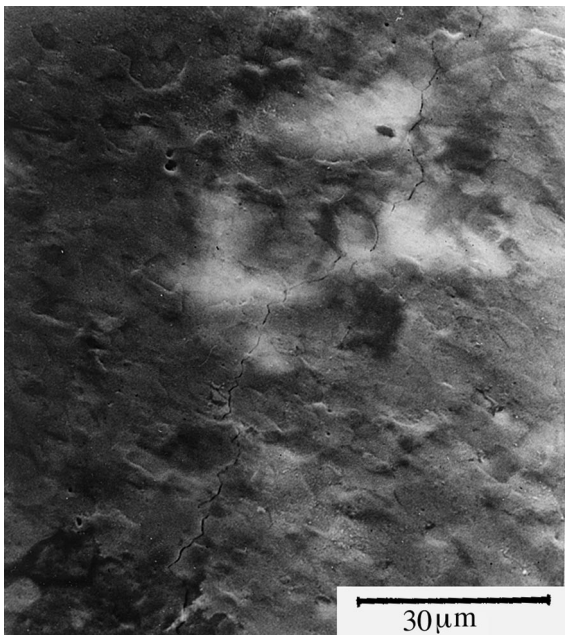

Fig. 20. SEM micrograph of a RXA specimen (M31) shows a large crack on the oxide surface.

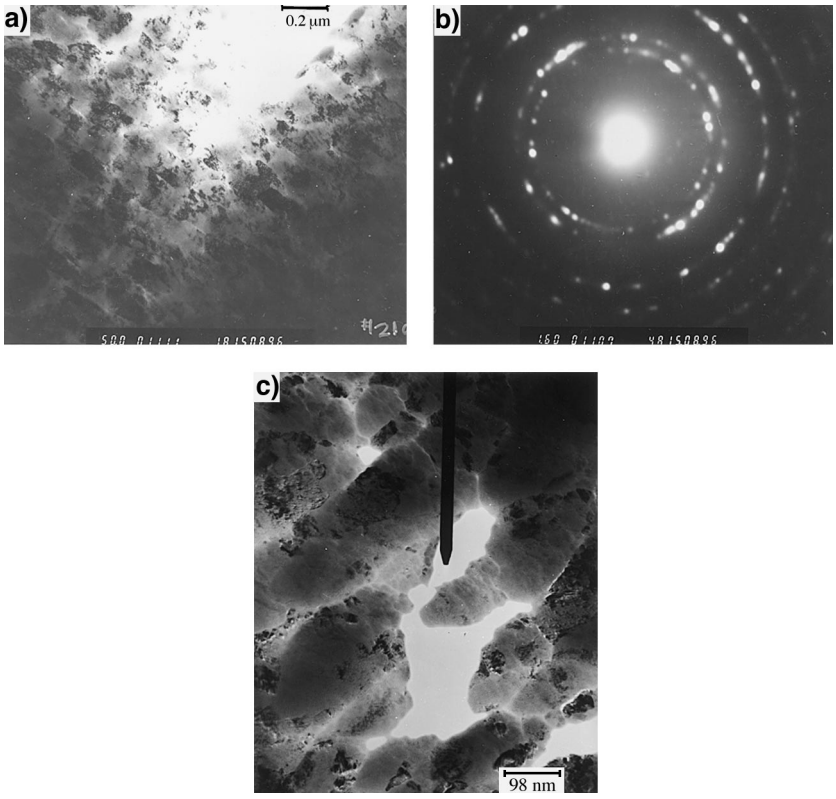

Fig. 21. TEM micrographs of oxide crystallites near the oxide/metal interface of a specimen autoclaved in LiOH/F^- solution with an hydrogen overpressure (M34). (a) Bright field, (b) diffraction pattern from (a), (c) enlarged view of a similar area to that in (a) taken on a different TEM (JEOL). Some evidence for porosity is seen even without using Fresnel contrast.

reduced pre-transition corrosion in both the pH7 and pH12 LiOH, and delayed transition, but had no effect on the long-term post-transition corrosion after >1000 days, which was, if anything, slightly worse after the α-anneal. In pH12 LiOH (Fig. 5) there was essentially no improvement in post-transition corrosion rate either and the α-annealed specimens performed worse during the excursion than the original β-quenched specimens. The continuation of the data beyond those in Fig. 5 shows that the wrong conclusion could have been reached about effects in pH7 water if only the data in Fig. 5 had been available.

When surface preparation differences were compared the effects appeared to be minimal for standard SRA Zircaloy-4. However, large differences in weight gain were evident for a late β-quenched batch (R), but post-transition curves tended to be parallel (and hence corrosion rates were very similar). Initial pre-transition weight gains were less for both flash- and fully-electropolished surfaces than for pickled surfaces. This relative behaviour was reversed for post-transition corrosion, with fully electropolished samples showing higher weight gains than flash- electropolished ones, both of which were significantly higher than for pickled specimens.

Under different oxidation conditions, lower pre-transition corrosion rates for electropolished compared with pickled surfaces have long been known to be the rule [44], as has the changeover in relative behaviour during post-transition corrosion. This was initially claimed to be a detrimental effect of fluoride remaining from the pickling process. This was shown not to be the explanation when electropolished surfaces were contaminated by a quick dip in a fluoride solution [45]. SEM examination showed the explanation to be an effect of dissolving all the intermetallic particles in the specimen surface during electropolishing [46]. This significantly reduces the number of available sites for the cathodic component of the oxidation reaction, which initially becomes rate limiting as a result of this. As the oxide thickens, initially subsurface intermetallics reach the oxide/metal interface and restore the local conductivity of the oxide from diffusion of their iron content [47]. It is believed that a similar effect was operating here. Intermetallic particles were removed from the surface during electropolishing (more effectively from the fully electropolished surfaces than from the flash electropolished surfaces) thus leaving the fewest intermetallic sites in the fully electropolished surfaces.

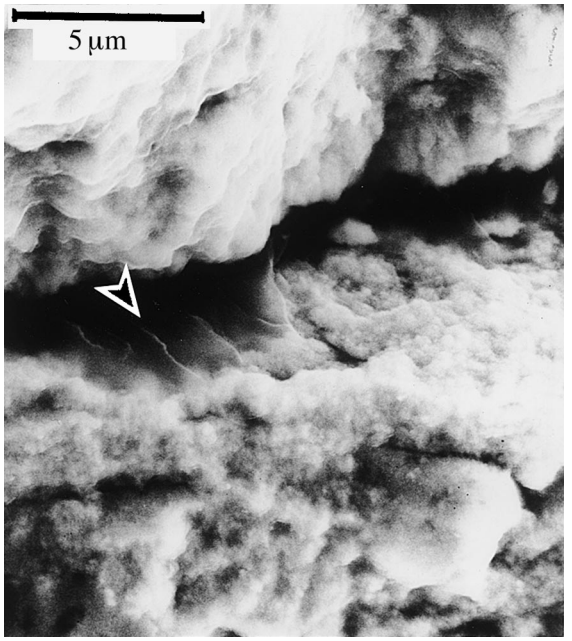

Fig. 22. Cross section of the fractured oxide (S30) showing evidence of large single crystals (river patterns, characteristic of cleavage of a single crystal are indicated by the arrow). The principal direction of the fracture surface is normal to the oxide/metal interface, and the crack containing the fractured crystal is roughly parallel to the specimen surface. It appears that when the oxide film was fractured a large single crystal which happened to be present along the crack path was also cleaved. The smaller particle below the crack which pulled out of the opposite fracture face did not fracture.

Pickling left many intermetallics as discrete local particles in the initial surfaces, whereas belt-grinding smeared out the intermetallics in the surfaces resulting in the most efficient distribution of the Fe over the initial surface and, hence, leading to the lowest post-transition oxidation rates.

Hydrogen analyses performed on a small number of specimens from this programme did not lead to any very significant conclusions. Numbers of analyses were small, and scatter was large enough that no major conclusions emerged. It appeared that the lower corrosion rates of the low-Sn material did not translate into noticeable reductions in end of life hydrogen contents and the high corrosion rates of β-quenched batches resulted in only small increases in end-of-life hydrogen contents (Tables 2 and 3). Analyses performed both with and without the oxide remaining on the specimens suggested that hydrogen concentrations in the oxide were very similar to those in the metal, so that the specimen preparation technique prior to hydrogen analysis did not materially affect the result for isothermally oxidized specimens in laboratory corrosion tests.

4.2. Oxide film examinations

Fig. 27 shows weight gains for a set of specimens from this project that were examined in detail. Before the F^- addition at 90 days all specimens had oxidized to about their transition thickness of 2 μm (although some very local spalling was evident on a few specimens). This thermally grown pre-transition oxide layer is a relatively protective dense oxide layer, as is apparent from the plateau in the oxidation kinetic curves and this film is under compressive stress because the new oxide layers are formed by inward migration of oxygen alone (the ratio of the unconstrained volume of the oxide to the volume of the metal from which it formed is approximately 1.56). After 30 days oxidation in the LiOH/ F^- solution, the specimens in solutions with H_2 overpres-

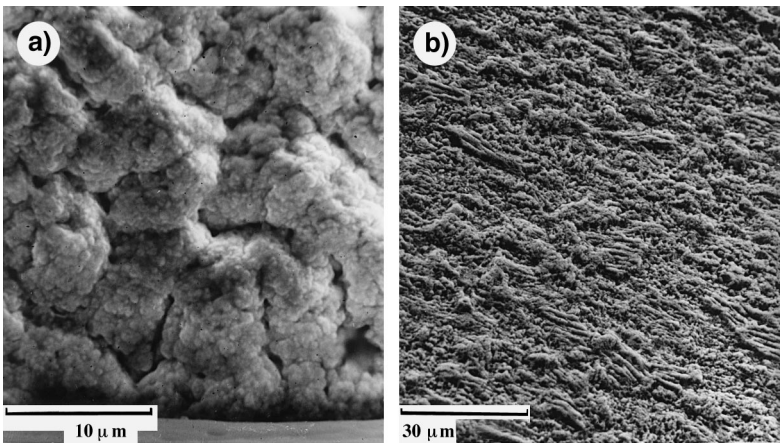

Fig. 23. (a) The oxide/metal interface of a specimen (S30) autoclaved with an hydrogen overpressure showed 'cauliflower-like' features. (b) The oxide/metal interface of a RXA specimen (M36) autoclaved in LiOH/F^- solution with an oxygen overpressure showed diffusional growth features associated with the metal matrix structure.

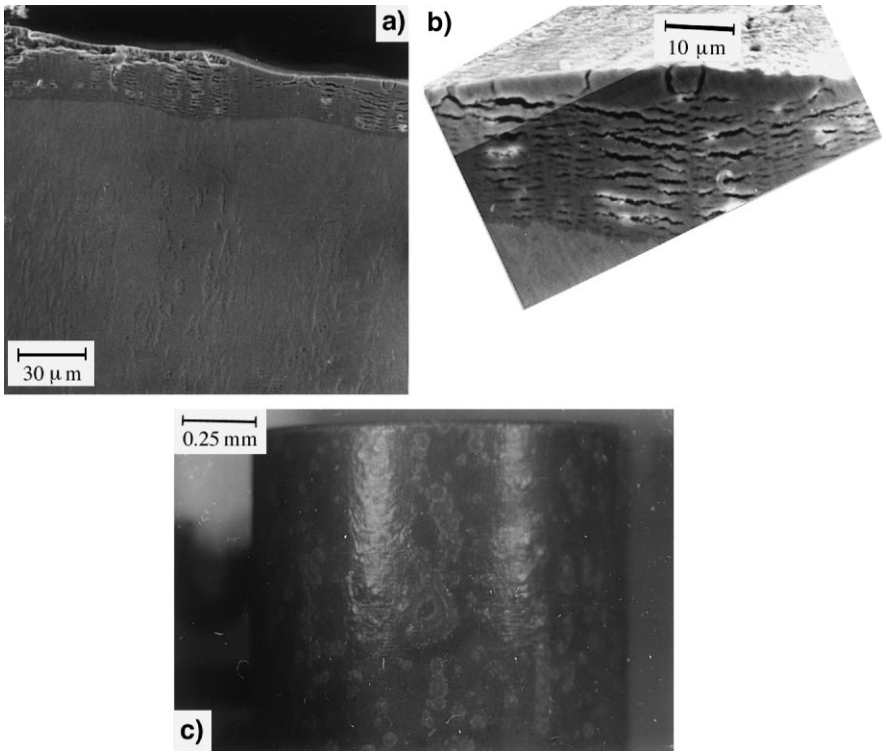

Fig. 24. (a) Cross section of an original specimen (S18) oxidised in 360°C pH12 LiOH solution without deliberate F^- additions (92 days) showing lateral crack patterns in the oxide layer. (b) Enlarged view of the oxide on the right of (a). (c) The pustular appearance of the specimen oxide surface.

sures had grown very thick porous oxide layers beneath the pre-transition layer as deduced from capacitance measurements (Fig. 13) and the different fractured appearance of the two layers in Fig. 14.

The bond between the outer oxide layer and the inner porous oxide appears to be very weak, and this bond cannot sustain the compressive stresses within the denser pre-transition layer. The effective Young's modulus for a thermally grown oxide film on a zirconium alloy is measured to be ~65 GPa for a thickness between 2 and 3.5 μm [48]. Therefore the layers first crack laterally (Figs. 20 and 24) and then separate locally to form surface blisters (Fig. 16) if the outer layer is able to buckle as in the β-quenched and SRA specimens. Long cracks with evidence of lateral cracking (charging areas in Fig. 20) were formed in RXA specimens. Formation of surface blisters rather than only long cracks (both vertical and lateral) is thought to depend on the mechanical strength of the outer (pre-transition) oxide layer. The formation of a blister, however, provides a much larger relatively closed volume in which hydrothermal reactions can proceed. The specimens oxidized in the solution with the high oxygen overpressure remained near to their transition thickness after the same test duration. The results in the 'high' hydrogen overpressure conditions showed weight gains and oxide thicknesses less than for those in the solution with the low hydrogen overpressure, probably because a leak in the autoclave allowed most of the hydrogen overpressure to escape. In the absence of a thick initial oxide (on specimens suffering spontaneous excursions) the formation of definite blisters was unfavourable, but pustules consisting of local layers of multiple cracks were formed instead (Fig. 24).

Information about the interconnection of the pores in the oxide was obtained from impedance spectroscopy measurements made after the oxides had been soaked with electrolyte. In many $\log Z$ vs. $\log f$ impedance plots it was observed that $\log Z$ has an approximately linear dependence on the logarithm of the frequency. The oxide films grown in the solution with the high oxygen overpressure generally have a near perfect capacitive character (with slopes for the $\log Z$ vs. $\log f$ plots between −0.9 and −1.0 in Table 5) which indicates that the oxide layer is very compact. Most of the specimens oxidized in the solution with the low oxygen overpressure also showed a good capacitive character, except for the RXA specimen (P33) for which the measured slopes were down to −0.88 (Table 5). The deviations from perfect capacitive behaviour indicate the existence of

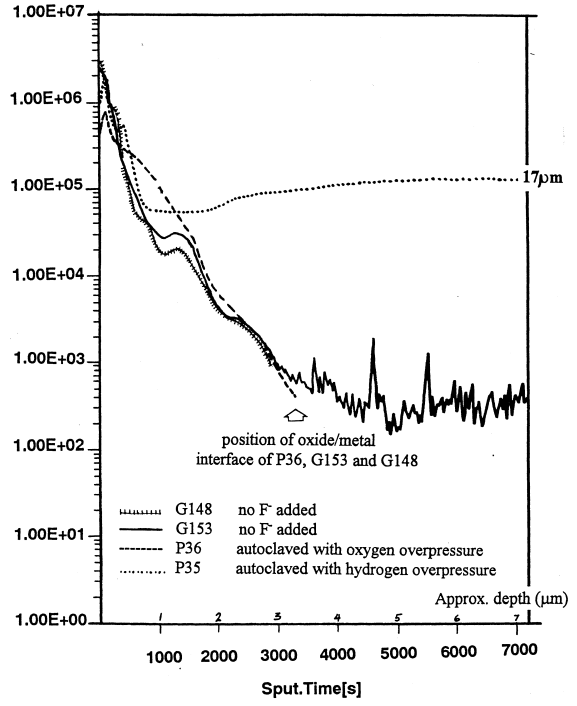

Fig. 25. SIMS profiles of ^{19}F in oxide films on Zircaloy-4 specimens.

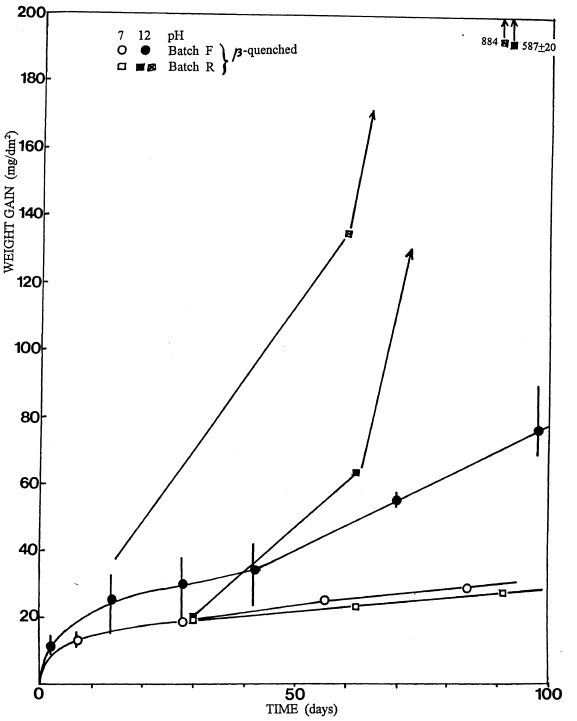

Fig. 26. Effect of the length of the initial autoclave cycle on the pre-transition corrosion of pickled specimens in pH12 LiOH (late β-quenched Zircaloy-4, batches F and R).

conducting channels in the bulk oxide, and so suggest that a number of pores exist inside the oxide film.

None of the specimens from the high hydrogen overpressure autoclave (which leaked) showed surface blisters, but the weight gains and FTIR interferometry indicated very thick oxide layers, and capacitance measurements showed that these oxides were very porous. The log Z vs. log f plots for these specimens have slopes ranging from −0.55 to −0.50 which implies a Warburg type impedance behaviour [49,50]. A Warburg type impedance is characteristic of diffusional 'transmission lines' and so these plots indicate the existence of long approximately one dimensional conductive channels (long pores soaked with electrolyte) in these oxides. The specimens oxidized in solution with the low hydrogen overpressure (the thickest oxides) had log Z vs. log f slopes ranging from −0.47 to− 0.33. This suggests the existence of three dimensional networks of laterally interconnected vertical pores. This type of oxide can be correlated, from log Z vs. log f plots, with the blistering phenomenon. For the oxides with the lowest slopes the vertical pores inside the bulk oxide become more interconnected, that is, there is more extensive porosity inside the bulk oxide. This contributes to the poor bonding of the inner oxide, which contains the networks of pores, to the initial dense outer oxide that causes the blistering of the outer oxide. Therefore the specimens that show the most surface blistering (S30, Fig. 19) and the most large surface cracks (M31, Fig. 20) have the lowest slopes for log Z vs. log f in Table 5 (−0.37 and −0.33, respectively).

During the course of the investigation, a number of observations indicated that hydrated zirconium oxide was being precipitated from solution during the oxide growth. The particulate deposits on the outer surface in Fig. 15(a) and the smeared appearance in Fig. 18(c) of the blister cap (when no corresponding smearing of the inner oxide occurred) both indicated the presence of a

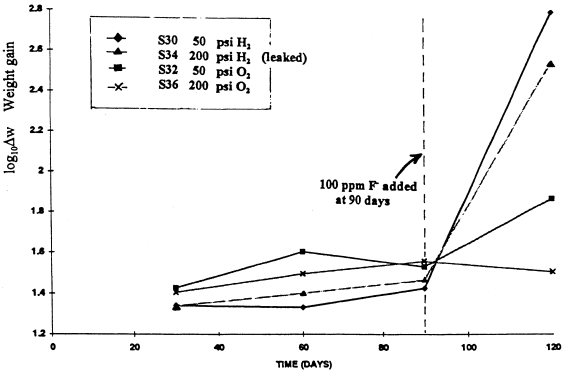

Fig. 27. Weight gain of low-tin Zircaloy-4 specimens heated in 360°C pH12 LiOH solution.

soft precipitate, which dissolved fairly easily in the nitric/HF etching solution or 50% nitric acid. EDX spectra showed only Zr peaks. The equiaxed particles found inside the blisters (Fig. 19) and the mismatch of the opposite topographies of the inner surface of the blister and the inner surface of its cap (Fig. 18) indicated the precipitation of ZrO_2 in a form which did not dissolve during a few hours immersion in the etching solution. Additional experiments [51] (not reported here in the interests of brevity) suggested that the particulates which are soluble in nitric acid are a form of hydrated zirconium oxide which is redeposited probably during cooling of the test solution enriched with the dissolved Zr compounds. The equiaxed particles are probably a dehydrated zirconium oxide, which is not readily soluble in either nitric acid or nitric/HF etching solution, and were probably formed during the autoclave test. Therefore hydrothermal dissolution and redeposition of ZrO_2 is suspected as the explanation of the observed features of the oxide films. This must happen inside the bulk of the oxide because there is no sign of topographical changes to the outer oxide surface, except for the deposition of the small particulates which were readily soluble in HNO_3/HF solution, and, therefore, must have formed during cooling of the autoclave.

When the metal was etched away from the oxide, the surface of the oxide/metal interface showed cauliflower-like features which could not be related to any metal matrix structures (Fig. 23(a)). These features are the contour of the oxidation front at the point where the autoclave test stopped. They formed right adjacent to the metal surface and there would always be a thin remaining barrier oxide layer on the zirconium metal surface because of the high affinity of zirconium for oxygen. From the impedance measurements, the presence of long channels of pores was inferred, and the cauliflower features are thought to represent the bottoms of bundles of pores approaching close to the oxide/metal interface (Fig. 28). These observations also suggest that the rate of oxidation depends on the rate of propagation of these pores, i.e. on the rate of dissolution of the ZrO_2 at the bottoms of the pores.

When the oxide film was fractured mechanically the presence of apparently large oxide single crystals was found (Fig. 22). The appearance was identical to the fractures of large oxide crystals observed in thick oxides formed at 650°C [35]. These crystals were bridging across large cracks that appeared to have been present prior to the fracturing of the sample. The occurrence of an oxide 'dissolution and reprecipitation' process was confirmed by these observations since it is difficult to conceive of another mechanism for forming such a crystal within a lateral crack that was already present in the oxide. Large equiaxed oxide single crystals embedded in the bulk oxide with a generally small crystallite size and within large cracks are not seen in thick post-transition oxide films grown in steam at 400°C or water at 300–360°C [52], but have been seen in thick degraded oxides grown in LiOH solutions at 350°C and in-reactor [21]. They also become more prevalent in oxides grown at much higher temperature on Zircaloy-2, whereas under the same conditions very large columnar oxide crystals (0.5 × 8 μm) form on Zr [35].

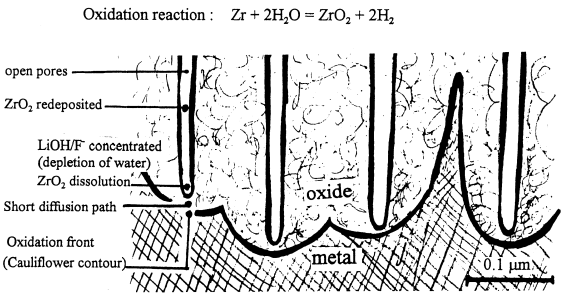

Fig. 28. Schematic representation of the cross section of the oxide/metal interface region of the oxide films on specimens autoclaved in LiOH/F^- solution with hydrogen overpressures, showing open pores, barrier oxide layer and the contour line of the cauliflower oxidation front. Lateral cracks interconnect the pores at higher elevations in the oxide.

TEM examinations of the oxide from the specimen oxidized in the solution with the high oxygen overpressure showed small crystallites with a size of approximately 10–40 nm and the diffraction patterns obtained are typical of m-ZrO_2. The 'spotty ring' diffraction pattern in Fig. 21(b) indicates that the crystallite sizes from the oxide grown in solutions with hydrogen overpressures are small and consistent with the crystallite sizes seen in Fig. 21(a). The bright field micrographs (Fig. 21(a) and (c)) show features of a size (<0.2 μm) and an elongated shape similar to the cauliflower-like features (the smallest resolvable features in Fig. 23(a)) seen at the oxide/metal interface. Similar cauliflower features have been reported from the corrosion films grown in-reactor on Zircaloy-4 [53].

4.3. A mechanism for the dissolution and redeposition process

Cox and Wu [6–8] have shown that even thin "pre-transition" ZrO_2 films grown in concentrated LiOH solution or in pH7 water contain fine pores. For the latter case, pores are found only on intermetallics. These pores are generated by an oxide dissolution process and would provide easy paths for the initial F^- penetration to the oxide/metal interface. At the oxide/metal interface at the bottom of such a pore, the oxidation reaction ($Zr + 2\ H_2O = ZrO_2 + 2\ H_2$) occurs as the water molecules are dissociated and O^{2-} ions reach the metal by diffusion through any thin oxide layer persisting at the bottom of the pore. As the oxidation reaction advances

and H_2O in the pore is depleted, the LiOH/F^- solution concentration could rise at the bottom of the pores. Under the reducing potential of the medium (with the hydrogen overpressure) and at some critical LiOH/F^- concentration, it is believed that stable Li_2ZrF_6/Li_2ZrOF_4 complexes are formed [37]. The anions ZrF_6^{2-}, $ZrOF_4^{2-}$ are very stable in F^- solutions at high temperatures and the hydrogen overpressure ensures the persistence of the required negative charge on the fluoride containing anions, keeping them from being oxidized [37,38]. However, the stability of the Li_2ZrF_6/Li_2ZrOF_4 complexes is very sensitive to the particular F^- concentrations because of the small size and low charge of the cation, Li^+, which cannot bind very strongly to the anions. Therefore these complexes, where there is a large hydrolysis constant, would easily hydrolyze [38,39].

Thus, the solubility of the ZrO_2 will increase with increasing F^- concentration and the O^{2-} diffusion paths through the residual barrier oxide at the bottoms of the pores are shortened by the continuous thinning of this barrier oxide layer. The rate of oxidation remains high because the residual oxide at the oxide/metal interface remains very thin (a few nm thick). From the vicinity of the oxide/metal interface, the Li_2ZrF_6/Li_2ZrOF_4 species in solution diffuse out through the porous bulk oxide. F^- concentration in the bulk solution is too low to maintain the stability of these species (also the hydroxide ion concentration in the bulk solution exceeds that of F^-). The hydrolysis reaction therefore becomes favorable in the bulk porous oxide and ZrO_2 is redeposited in the large cracks in the porous layer (Fig. 22) or inside blisters that develop (Fig. 19).

The critical factor leading to ZrO_2 degradation in a LiOH/F^- aqueous environment is believed to be the good complexing ability of the solution [37]. The complexing ability of the solution controls the dissolution of the ZrO_2. This scenario of a dissolution and reprecipitation process of oxides in alkali/F^- aqueous solutions is a well known procedure for growing single crystals of refractory materials known as the Hydrothermal Crystal Growth method. Refractory metal oxide crystals have very high melting points, and are difficult to grow by other methods such as the molten salt method [37].

4.4. Effect of the oxygen overpressure

If F^- is the main complexing agent for the dissolution process, and if fluoride were to be driven out of the aqueous environment, the degradation process would cease: Consider the following reaction

$$2F^- + O_2 + H_2O = F_2O + 2OH^-.$$

For excess O_2, the reaction proceeds to right consuming F^- to form F_2O. F_2O has a very low boiling point (−50°C), keeping its concentration low in an aqueous environment. SIMS profiles showed that in fact the F^- concentration in the oxides grown with high O_2 overpressures were no higher than those observed for pickled surfaces not exposed to any added F^- in the solution (Fig. 25) and were lower at the oxide surface. Since fluoride left on the specimen surface after pickling is incorporated into the surface oxide layers during the initial oxidation, it is, perhaps, not surprising that O_2 overpressures (which will oxidize F^- in solution, but leave F^- already incorporated in the oxide unaffected) cannot eliminate all this F^-. In contrast, oxides grown in the solution with the high hydrogen overpressure have high uniform F^- concentrations throughout the bulk of the oxide (Fig. 25). It is thought that either F_2O or F_2 (also volatile) formed inside the autoclaves with the O_2 overpressures and thereby lowered the F^- concentration in the pores in the oxide film. Thus, the oxide on the specimens in the solution with a 200 psi O_2 overpressure were not degraded by the addition of F^- to the autoclave. However, the oxide on some of the specimens in the autoclave with only 50 psi O_2 overpressure show an array of very small blisters but showed no large oxidation rate excursions. This blistering probably occurred because the dissolved O_2 concentration was not high enough to form F_2O or F_2 rapidly and prevent an initial degradation effect. Eventually, enough of the F^- was consumed that a large oxidation excursion did not develop in the autoclave with the 50 psi O_2 overpressure.

5. Conclusions

Oxidation rate excursions that were observed when freshly prepared specimens were added to already operating autoclave tests in pH12 LiOH at 360°C are ascribed to a synergistic effect of LiOH and fluoride ion leached from the freshly pickled specimens that were added. No similar effect of adding fresh specimens was observed in pH7 water at 360°C.

- The standard Zircaloy metallurgical conditions tested were SRA, RXA and a late β-quench, (each of these conditions was given an additional 1 h anneal at 600°C). A low-tin SRA Zircaloy-4 was also tested. With one exception, all the metallurgical variations of Zircaloy-4 in the tests underwent excursions. The exception was a group of specimens given an (α + β) anneal and slow cool to simulate a weld heat-affected zone. This treatment was expected to result in poor corrosion resistance even in the absence of F^-, but did not. These samples, however, proved to be immune to degradation.
- The low-tin material appeared to be more sensitive to these synergistic effects than other materials, leading to the suspicion that this material may be more sensitive to other severe water chemistry conditions.
- Tests with deliberately added fluoride and either hydrogen or oxygen overpressures showed similar

excursions with hydrogen overpressures but not with oxygen overpressures. If fluoride can be oxidized to a volatile form in the highly oxidising conditions this could leach the fluoride from the specimen surfaces before it can lead to oxide degradation.

- The synergistic effects were a function of the amount of fluoride added (number of freshly pickled specimens) and the length of the autoclave cycle. Only cycles $\geqslant 60$ days, without shutdown and removal of the contaminated solution, led to severe excursions. Shorter cycles appeared to cause slightly increased pre-transition oxidation weight gains for some batches, but without the severity of the longer cycles.
- Examination of the oxide films formed during the corrosion rate excursions has elucidated a mechanism by which LiOH and fluoride can accelerate oxide growth. We have provided strong supporting evidence for the hypothesis that oxidation excursions in $LiOH/F^-$ solution under H_2 overpressure are caused by the degradation of the protective ZrO_2 film via an hydrothermal dissolution and redeposition process.
- $LiOH/F^-$ solution first penetrates into the bulk of the oxide through the pores that develop during the kinetic rate transition and this solution when concentrated in the pores is capable of forming stable complexes with ZrO_2 thus increasing the solubility of ZrO_2. Dissolved ZrO_2 recrystallized in the bulk porous oxide recycling F^- back into solution. Thus, the dissolution process catalyzes itself, causing runaway oxidation.
- The chemistry of the coolant, especially the $LiOH/F^-$ effect should be given more attention to ensure the satisfactory performance of reactor fuel cladding. In particular analyses of the oxides from reactor fuel cladding for F^- are recommended in order to establish whether any F^- formed in-reactor is strongly adsorbed in the oxide on the cladding. The only instance where such analyses have been performed was for non-pickled Zr–2.5%Nb CANDU pressure tubes [54], and here significant F^- concentrations were found in the oxide films.

Acknowledgements

The authors are grateful to the Natural Sciences and Engineering Research Council of Canada and the CANDU Owner's Group for the funding that allowed this research to be performed. Steve Bushby (AECL, Chalk River) kindly performed SIMS analyses of surface oxides. The Nuclear Fuel Industry Research (NFIR) Group kindly permitted this study of specimens from one of their programmes, and this publication of the results.

References

[1] B. Cox, What is wrong with current models for in-reactor corrosion, Proc. Tech. Comm. on Fundamental Aspects of Corrosion on Zirconium Base Alloys in Water Reactor Environments, Portland, OR, International Atomic Energy Agency, Vienna, IWGFPT34, 1990, pp. 167–173.
[2] D.R. Tice, G. Huddart, I.L. Bramwell, Corrosion of Zircaloy-4 fuel cladding in high concentration lithium and boron conditions simulating extended burnup in PWR, Proc. Conf. On Materials for Nuclear Core Application, British Nuclear Energy Soc. 1987, Paper 10.
[3] I.L. Bramwell, P.D. Parsons, D.R. Tice, in: C.M. Eucken, A.M. Garde (Eds.), Corrosion of Zircaloy-4 PWR Cladding in Lithiated and Borated Environments, Proc, 9th Int. Symp. on Zr in the Nuclear Industry, ASTM-STP-1132, American Society for Testing and Materials, Philadelphia, PA, 1991, pp. 628–642.
[4] R.A. Perkins, R.A. Busch, Corrosion of Zircaloy in the Presence of LiOH, ibid. pp. 595–612.
[5] G.P. Sabol, G.R. Kilp, M.G. Balfour, E. Roberts, in: L.F.P. van Swam, C.M. Eucken (Eds.), Development of a Cladding Alloy for High Burnup, Proc. 8th Int. Symp. on Zr in the Nuclear Industry, ASTM-STP-1023, American Society for Testing and Materials, Philadelphia, PA, 1989, pp. 227–244.
[6] B. Cox, C. Wu, J. Nucl. Mater. 199 (1993) 272.
[7] B. Cox, C. Wu, J. Nucl. Mater. 224 (1995) 169.
[8] B. Cox, M. Ungurelu, Y.-M. Wong, C. Wu, in: E.R. Bradley, G.P. Sabol (Eds.), Mechanisms of LiOH Degradation and H_3BO_3 Repair of ZrO_2 Films, Proc. 11th Int. Symp. on Zr in the Nuclear Industry, ASTM-STP-1295, American Society for Testing and Materials, W. Conshohocken, PA, 1996, pp. 114–136.
[9] Meeting the Demanding Nuclear Fuel Performance Challenges of the '90's – Westinghouse ZIRLO Products for PWR Fuel, Westinghouse Electric Corp., P.O. Box 355, Pittsburgh, PA, 1993.
[10] S.G. McDonald, G.P. Sabol, K.D. Sheppard, in: D.G. Franklin, R.B. Adamson (Eds.), Effect of Lithium Hydroxide on the Corrosion Behaviour of Zircaloy-4, Proc. 6th Int. Symp. on Zr in the Nuclear Industry, ASTM-STP-824, American Society for Testing and Materials, Philadelphia, PA, 1984, pp. 519–530.
[11] H. Coriou, L. Grall, J. Meunier, M. Pelras, H. Willermoz, J. Nucl. Mater. 7 (1962) 320.
[12] E. Hillner, J.N. Chirigos, The effect of lithium hydroxide and related solutions on the corrosion rate of Zircaloy-2 in 680°F water, US Report, WAPD-TM-307, Bettis Atomic Power Lab., Pittsburgh, PA, 1962.
[13] S. Kass, Corrosion 25 (1969) 30.
[14] R.A. Murgatroyd, J. Winton, J. Nucl. Mater. 23 (1967) 249.
[15] A.V. Manolescu, P. Mayer, C.J. Simpson, Corrosion 38 (1982) 21.
[16] N. Ramasubramanian, N. Preocanin, V.C. Ling, in: L.F.P. van Swam, C.M. Eucken (Eds.), Lithium Uptake and the Accelerated Corrosion of Zirconium Alloys, Proc. 8th Int. Symp. on Zr in the Nuclear Industry, ASTM-STP-1023, American Society for Testing and Materials, Philadelphia, PA, 1989, pp. 187–201.

[17] S. Somiya, Hydrothermal Reactions for Materials Science and Engineering, Elsevier, London, 1989.
[18] B. Cox, Y.-M. Wong, in: C.M. Eucken, A.M. Garde (Eds.), Effect of LiOH on pretransition zirconium oxide films, Proc. 9th Int. Symp. on Zr in the Nuclear Industry, ASTM-STP-1132, American Society for Testing and Materials, Philadelphia, PA, 1991, pp. 643–662.
[19] B. Cox, C. Wu, in: B.R. MacDougall, R.S. Alwitt, T.A. Ramanarayanan (Eds.), Degradation of Zirconium Oxide Films in LiOH, Proc. Symp. on Oxide Films on Metals and Alloys, Proc. vol. 92-22, Electrochemical Soc., Pennington, NY, 1992, pp. 265–279.
[20] X. Iltis, F. Lefebvre, C. Lemaignan, J. Nucl. Mater. 224 (1995), 109 and 121.
[21] X. Iltis, F. Lefebvre, C. Lemaignan, in: E.R. Bradley, G.P. Sabol (Eds.), Microstructure Evolutions and Iron Redistribution in Zircaloy Oxide Layers: Comparative Effects of Neutron Irradiation Flux and Irradiation Damages, Proc. 11th Int. Symp. on Zr in the Nuclear Industry, ASTM-STP-1295, American Society for Testing and Materials, W. Conshohocken, PA, 1996, pp. 242–264.
[22] B. Cox, J. Nucl. Mater. 249 (1997) 87.
[23] S. Kass, Corrosion 16 (1960) 93t.
[24] S. Kass, Corrosion 17 (1961) 566t.
[25] E. Hillner, H.D. Cook, Fluorine content of Zircaloy corrosion films, US Report, WAPD-T-1639, Bettis Atomic Power Lab., W. Mifflin, Pa, 1963.
[26] F.H. Krenz, A preliminary study of the effect of added fluoride on the corrosion of Zr-2 in water at 300°C, Canadian Report, AECL-1507, Atomic Energy of Canada Ltd., Chalk River, 1962.
[27] W.E. Berry, Effect of Fluoride Ions on the Aqueous Corrosion of Zirconium Alloys, Proc. Symp. on Corrosion of Zirconium Alloys, ASTM-STP-368, American Society for Testing and Materials, Philadelphia, PA, 1964, pp. 28–40.
[28] B. Cox, Y.-M. Wong, P. Dume, J. Nucl. Mater. 250 (1997) 200.
[29] L.F.P. van Swam, S.H. Shann, Corrosion of Zircaloy-4 fuel cladding in pressurized water reactors, in: C.M. Eucken, A.M. Garde (Eds.), Proc. 9th Int. Symp. on Zr in the Nuclear Industry, ASTM-STP-1132, American Society for Testing and Materials, Philadelphia, PA, 1991, pp. 758–781.
[30] B. Cox, N. Ramasubramanian, V.C. Ling, Zircaloy corrosion properties under LWR coolant conditions (Part I), Report EPRI-NP6979D, Electric Power Research Inst., Palo Alto, CA 94304, October 1990, USA.
[31] L.G. Bell, The effect of oxygen on the hydriding rate of Zircaloy-2 in LiOH solution, Canadian Report, HSEN-FCP-67-003, Hawker Siddeley Engineering, Malton, Ontario, 1967.
[32] B. Cox, Y.-M. Wong, J. Nucl. Mater. 199 (1993) 258.
[33] B. Cox, The use of electrical methods for investigating the growth and breakdown of oxide films on Zirconium alloys, Canadian Report AECL-2668, Atomic Energy of Canada Ltd., Chalk River, 1967.
[34] B. Cox, J. Aust. Inst. Met. 14 (1969) 123.
[35] B. Cox, A. Donner, J. Nucl. Mater. 47 (1973) 72.
[36] H.R. Peters, in: D.G. Franklin, R.B. Adamson (Eds.), Improved Characterization of Aqueous Corrosion Kinetics of Zircaloy-4, Proc. 6th Int. Symp. on Zr in the Nuclear Industry, ASTM-STP-824, American Society for Testing and Materials, Philadelphia, PA, 1984, pp. 507–518.
[37] A.N. Lobachev, Crystallization Processes Under Hydrothermal Conditions, New York Consultants Bureau, Plenum, New York, 1973, p. 15 and p. 53.
[38] I.A. Sheka, A.A. Lastochkina, Russian J. Inorg. Chem. 6 (1961) 954.
[39] W.B. Blumenthal, The Chemical Behaviour of Zirconium, Nostrand, New York, 1958, p. 142.
[40] V. Vrtilkova, L. Molin, SKODA-Zbraslav, Prague, Czech Republic, private communication.
[41] B. Cox, C. Roy, Electrochem. Tech. 4 (1966) 123.
[42] B. Cox, J.P. Pemsler, J. Nucl. Mater. 28 (1968) 73.
[43] S. Kass, Development of the Zircaloys, Proc. of a Symposium on Corrosion of Zirconium Alloys, ASTM-STP-368, American Society for Testing and Materials, Philadelphia, PA, 1964, pp. 3–27.
[44] J.T. Demant, J.N. Wanklyn, The effects of contamination on the oxidation of Zirconium in steam, UKAEA Report AERE-R4788, 1965.
[45] B. Cox, Oxidation of Zirconium and its alloys, in: M.G. Fontana, R.W. Staehle (Eds.), Adv. in Corr. Sci. and Tech., vol. 5, Plenum, New York, 1976, pp. 173–391.
[46] IAEA TECDOC-996, Waterside Corrosion of Zirconium Alloys in Nuclear Power Plants, International Atomic Energy Agency, Vienna, 1998.
[47] B. Cox, H.I. Sheikh, J. Nucl. Mater. 249 (1997) 17.
[48] K.F. Amouzouvi, L.J. Clegg, Scr. Metall. Mater. 30 (1994) 1139.
[49] J. Ross Macdonald, Impedance Spectroscopy, Wiley, New York, London, 1987, pp. 2–6.
[50] D.D. Macdonald, Corrosion 46 (1990) 229.
[51] Y.-M. Wong, M.A.Sc. thesis, Department of Metallurgy and Materials Science, University of Toronto, 1997.
[52] B. Cox, Y. Yamaguchi, J. Nuclear Mater. 210 (1994) 303.
[53] O. Gebhardt, A. Hermann, G. Bart, H. Blank, F. Garzarolli, I.L.F. Ray, in: E.R. Bradley, G.P. Sabol (Eds.), Investigation of in-pile grown corrosion films on zirconium-based alloys, Zirconium in the Nuclear Industry, Eleventh International Symposium, ASTM STP1295, American Society for Testing and Materials, W. Conshohocken, 1996, pp. 218–241.
[54] N.S. McIntyre, C.G. Weisener, R.D. Davidson, J. Nucl. Mater. 178 (1991) 80.